71-15,347

WILSON, Stephen Scott, 1939-
ISOTOPIC SPIN INVARIANCE IN THE REACTION
n+p→ π° +d.

The University of Michigan, Ph.D., 1970
Physics, elementary particles

University Microfilms, A XEROX Company, Ann Arbor, Michigan

THIS DISSERTATION HAS BEEN MICROFILMED EXACTLY AS RECEIVED

ISOTOPIC SPIN INVARIANCE IN THE REACTION $n+p \rightarrow \pi^{\circ}+d$

by
Stephen Scott Wilson

A dissertation submitted in partial fulfillment
of the requirements for the degree of
Doctor of Philosophy
(Physics)
in The University of Michigan
1970

Doctoral Committee:
Professor Michael J. Longo, Chairman
Professor Lawrence W. Jones
Professor Robert R. Lewis
Professor Richard K. Osborn
Professor Oliver E. Overseth

ABSTRACT

ISOTOPIC SPIN INVARIANCE IN THE REACTION $n+p \rightarrow \pi^{o}+d$

by

Stephen Scott Wilson

Chairman: Michael J. Longo

A measurement of the differential cross sections for the reaction $n+p \rightarrow \pi^{o}+d$ has been made at the Lawrence Radiation Laboratory 184-inch cyclotron. A neutron beam with kinetic energies up to 720 MeV was incident on a liquid hydrogen target. The angle and momentum of the deuterons were measured using an analyzing magnet and wire spark chambers with a magnetostrictive readout system. The photons from the decaying π^{o} were not detected. The neutron energy was calculated from the measured deuteron angle and momentum.

Out of 5×10^{5} events recorded, 1.1×10^{5} events were the desired $\pi^{o}+d$ reaction. The cross sections were compared to that for the reaction $\pi^{+}+d \rightarrow p+p$ as a test of isotopic spin invariance in strong interactions. We investigated the asymmetry of our cross sections and find agreement with isospin invariance to about 0.7% accuracy.

ACKNOWLEDGEMENTS

I would like to thank my advisor, Dr. Michael Longo, for suggesting the topic of this thesis and encouraging me to pursue it.

I am grateful to Bryce Schrock and the Lawrence Radiation Laboratory programmers for their valuable assistance in the data analysis.

The experimental design and set-up involved the collaboration of many people. Among those are David Cheng, Victor Perez-Mendez, Leonard Proehl, and John Sperende from LRL; Roy Haddock, Jerome Helland, and Bryce Schrock from UCLA; and Kenneth Young and Michael Longo from U of M. The 184-inch Cyclotron crew gave us excellent support throughout the experiment.

I am grateful to Orman Hass and Ralph Smith for helping build the spark chambers.

Finally I would like to thank my wife Kathy for enduring my interest in high energy physics (which is a conspiracy against domestic life). She enthusiastically proofread and typed the manuscript.

TABLE OF CONTENTS

	Page
ACKNOWLEDGMENTS	ii
LIST OF ILLUSTRATIONS	iv
LIST OF TABLES	v
I. INTRODUCTION	1
A. Objectives	1
B. Isotopic Spin Invariance	2
C. Consequences of Isospin Invariance for This Experiment	3
D. General Consequences of Isospin Invariance	5
E. Theory of Pionic Disintegration of the Deuteron	6
II. EXPERIMENTAL APPARATUS	8
A. General Description	8
B. Neutron Beam	10
C. Hydrogen Target	12
D. Magnetostrictive Readout System	12
E. Spark Chamber Construction	16
F. Spectrometer	19
G. Counters	20
H. Logic	20
III. DATA ANALYSIS	23
A. Location of Sparks	23
B. Alignment Checks	25
C. Momentum Determination	26
D. Solid Angle Calculation	29
E. Data Processing and Binning	31
F. Separation of Deuterons and Protons	34
G. Corrections to Data	36
H. Cross Section Calculation	40
IV. RESULTS	44
A. Cross Section	44
B. Systematic Errors	44
C. Coefficients	54
D. Comparison with Other Experiments	56
E. Total Cross Section	57
F. Comparison with Theory	57
V. CONCLUSIONS	61
LIST OF REFERENCES	62

LIST OF ILLUSTRATIONS

Figure		Page
1	Floor plan	9
2	Neutron energy distribution	11
3	Beam profile	11
4	Target	13
5	Wire chamber schematic	15
6	Magnetostrictive delay line	15
7	MS wire strain vs. distance	15
8	Chambers 3 and 4	17
9	Chambers 1 and 2	18
10	Deuterons covered by spectrometer	21
11	Geometry of orbits	27
12	Typical histograms for the time of flight	33
13	Momentum loss of deuteron	39
14	Deuteron loss from nuclear collisions	39
15	Laboratory phase space	43
16	Differential cross section at 325 MeV	46
17	Differential cross section at 375 MeV	47
18	Differential cross section at 425 MeV	48
19	Differential cross section at 475 MeV	49
20	Differential cross section at 525 Mev	50
21	Differential cross section at 575 Mev	51
22	Differential cross section at 625 Mev	52
23	Differential cross section at 675 MeV	53
24	Coefficients	55
25	Total cross section	58

LIST OF TABLES

Table		Page
1	Number of Events us. Number of Sparks	19
2	Mortality Rate of Events	32
3	Disposition of Events (in thousands)	36
4	Angular Distributions Normalized to an Area 2π x 1000	45
5	Coefficients	56
6	Maximum Violation with 90% Confidence Level	57
7	Coefficients of Shiff et. al.	59

I. INTRODUCTION

I-A. Objectives

This thesis will describe an experimental study of the reaction $n+p \rightarrow \pi^0+d$ and its significance as a test of isotopic spin invariance in strong interactions. The primary objective in setting up the experiment was to test time reversal invariance in the photodisintegration of the deuteron by measuring cross sections for the reaction $n+p \rightarrow \gamma+d$[1]; but, with little extra effort, about 5×10^5 events were recorded to obtain cross sections for $n+p \rightarrow \pi^0+d$ from threshold to 720 MeV incident neutron energy. The experiments were carried out at the Lawrence Radiation Laboratory (LRL) 184-inch cyclotron.

The cross section for π^0+d production is about 100 times larger than that for $\gamma+d$ production. To discriminate between these two reactions, the $\gamma+d$ experiment had to measure the deuteron trajectory and momentum using spark chambers and a magnetic spectrometer, and also the gamma trajectory using a multiple gap spark chamber that would detect the gamma by creating a secondary shower. The gamma chamber array could also detect one of the gammas coming from the decaying π^0. In the data analysis, the two reactions could be separated using kinematics to distinguish $\gamma+d$ production from π^0+d production.

It would have been possible to obtain the π^0+d cross section simply by using the enormous number of events rejected by the $\gamma+d$ experiment. This was not done because the gamma chambers were not necessary for the π^0+d cross section. Inclusion of the gamma chambers would have made the data analysis much more diffucult. The calculation of the solid angle of the detectors would have required an accurate and extensive Monte Carlo calculation. We would also have needed a detailed know-

ledge of the efficiency of the gamma detector down to about 50 Mev.

It was much easier to obtain the $d+\pi^o$ cross section by making separate runs where the gamma chambers were not used, and the event was recorded when only a deuteron was detected. The total event rate in this mode was as high as five events per second and was limited by the recovery time of the spark chambers. The total running time was about four days. With the simple trigger logic used, about half the events were protons coming from elastic and inelastic collisions rather than deuterons. For particles of the same momentum, the time of flight information (recorded with a time-to-height system) was used to separate the deuterons from the faster moving protons.

Isotopic spin invariance requires that the cross section for the reaction $n+p \rightarrow \pi^o+d$ must be half of that for $p+p \rightarrow \pi^+ +d$ as pointed out by Yang in 1952 (unpublished); i.e.

$$\frac{\sigma(pp\rightarrow\pi^+ d)}{\sigma(np\rightarrow\pi^o d)} = 2. \qquad (1)$$

To test for invariance, we can compare the cross section from our experiment with that from $p+p \rightarrow \pi^+ +d$ experiments, (or $\pi+d \rightarrow p+p$ experiments.) In particular, the differential cross section for $n+p \rightarrow \pi^o+d$ must be symmetric about 90° in the center of mass system as is that for $p+p \rightarrow \pi^+ +d$.

I-B. Isotopic Spin Invariance

Shortly after the neutron was discovered, it was found that it seemed to have the same strong forces as the proton: for particles in the same state, the forces between two protons, two neutrons or a proton and a neutron, were about the same after Coulomb effects were taken into consideration. These observations led to the conjecture that the strong

forces are identical (charge independent), and that the neutron and proton are two different "states" of the same particle, the nucleon. These states are distinguished by the orientation of their "isotopic spin", or "isospin", which is analogous to ordinary spin.

The total isospin of a nucleon is I = 1/2. It is in the proton or neutron state depending on whether the I_3 component of I is +1/2 or -1/2 respectively. Experimental evidence indicates that pions can also be represented as isospin states. The pion has a total isospin I = 1. The three possible I_3 components, +1, 0, -1, correspond respectively to the π^+, π^o, π^-.

The concept of charge independence can be stated in the language of isospin: if the initial and final states of a strong interaction are represented as eigenstates of total isospin, then the interaction is independent of I_3. This independence is mathematically analogous to rotational invariance in ordinary space. Thus, as for angular momentum, there will be a law of conservation of total iosospin.

I-C. Consequence of Isospin Invariance for This Experiment

Equation 1 can be derived using the methods developed for handling angular momentum. The two nucleon state can be written as $|i, i_3, i', i_3'\rangle$. Since the deuteron has zero isospin, the final state is written as $|I,I_3\rangle$. The initial states can be written as eigenstates of total isospin:

$$\text{np:}\quad |\tfrac{1}{2},-\tfrac{1}{2},\tfrac{1}{2},+\tfrac{1}{2}\rangle = \sqrt{\tfrac{1}{2}}\,|1,0\rangle + \sqrt{\tfrac{1}{2}}\,|0,0\rangle$$

$$\text{pp:}\quad |\tfrac{1}{2},+\tfrac{1}{2},\tfrac{1}{2},+\tfrac{1}{2}\rangle = |1,1\rangle$$

With a scattering matrix S, the ratio of the cross sections becomes:

$$\frac{|\langle \psi_{\pi\cdot d}|S|\psi_{pp}\rangle|^2}{|\langle \psi_{\pi\cdot d}|S|\psi_{np}\rangle|^2} = \frac{|\langle 1,1|S|1,1\rangle|^2}{|\,\tfrac{1}{\sqrt{2}}\langle 1,0|S|1,0\rangle + \tfrac{1}{\sqrt{2}}\langle 1,0|S|0,0\rangle\,|^2} \qquad (2)$$

Since the second term in the denominator does not conserve isospin, it must vanish. Since strong forces are independent of the third component of isospin,

$$\langle 1,1|S|1,1\rangle = \langle 1,0|S|1,0\rangle \ ,$$

the amplitudes in the numerator and denominator cancel leaving a factor of two.

There are three consequences which we specifically investigate:

1. The shape of the angular distribution for this experiment should be the same as that for other $N+N \rightleftarrows \pi+d$ experiments. Thus we fit our angular distributions to the function

$$\sigma(\theta) \sim A + \cos^2\theta + B \cos^4\theta$$

and compare the measured values of A and B with those from other experiments. This check depends on the relation

$$\langle 1,1|S|1,1\rangle = \langle 1,0|S|1,0\rangle,$$

and is therefore sensitive to a violation of the invariance of the strong force with respect to I_3.

2. Our angular distributions should be symmetric about 90° as they are for $p+p \rightarrow \pi^+ + d$, (because of the identity of the two protons in the initial state). Thus, we check the size of the asymmetry of our angular distributions. This test does not require knowledge of the results of other $N+N \rightleftarrows \pi+d$ experiments.

This test is sensitive to the requirement that total isospin is conserved; namely $\langle 1,0|S|0,0\rangle = 0$ in Equation 2. If this transition were not zero, it would give rise to odd powers of $\cos\theta$, whereas the $\langle 1,0|S|1,0\rangle$ transition gives rise only to even powers of $\cos\theta$. This point is discussed further in Sections I-E and IV-F.

3. The total cross section for our experiment should have the same energy dependence as that for the other $N+N \rightleftarrows \pi+d$ experiments. We have made this check, but it is not very accurate.

These three checks could possibly show violations due to the electromagnetic interaction, but there has been no theoretical work done to calculate the size and nature of the EM violation. Furthermore, the EM violation would be expected to be small since there are no Coulomb forces in either the initial or final states of the reaction $n+p \rightarrow \pi^o+d$, and the mass differences are small. However, we have not seen a violation in this experiment even at the 0.7% level; so the size of the EM violation is still an academic question.

Tests of isospin violation in other types of experiments are often more difficult because the EM corrections are considerably larger, ranging from 2 to 5%. This point is elaborated in the next section.

I-D. General Consequences of Isospin Invariance

Isospin invariance can be tested in a number of different areas. Examples of the best checks to date in the various areas are given in this section.

As an example of an application of isospin invariance to bound states, the excited levels of the mirror nuclei Li^7 and Be^7 are equal to within 2% to 4%[2]. The investigation of bound states to test isospin is difficult because of the large Coulomb corrections which are necessary.

In elastic scattering, the cross section for the scattering of a π^- off of a deuteron should be the same as that for a π^+. The cross sections have been measured to be equal within 0.75%[1,2]. However, this method only checks invariance with respect to the I_3 component; it does not check conservation of total isospin.

A number of experiments have been done involving pions and light nuclei. The reaction

$$d+d \rightarrow He^4+\pi^o$$

is forbidden because of isospin invariance. (The deuterons and He^4 have zero isospin whereas the pion has isospin one.) An experimental upper limit of its cross section has been measured by Poirier and Pripstein[3]. Greider[4] calculated from these results that isospin is conserved to at least 6.5%.

Isospin invariance requires that the cross section for

$$p+d \rightarrow \pi^+ + {}^3H \qquad \text{and}$$
$$p+d \rightarrow \pi^o + {}^3He$$

should have the ratio

$$\frac{\sigma({}^3H)}{\sigma({}^3He)} = 2 \ .$$

These reactions were measured by Crewe[5] at 450 Mev, and Hartig[6] at 591 Mev. Agreement was found within 13% and 5% accuracy respectively. This test involves a rather large and uncertain EM correction of about 6% since there is a large difference between the masses and wave functions of ${}^3H$ and ${}^3He$.

I-E. Theory of Pionic Disintegration of the Deuteron

There are a number of theoretical models for the reaction $N+N \rightleftarrows \pi+d$. The most successful is a covariant theory by D. Shiff and J. Tran Thanh Van who calculate the singularity structure of the scattering amplitude using Feynman diagrams, and then dispersion relations for the partial wave amplitudes[9]. They also give a summary of other models. The theories previous to this are unsatisfactory for our purposes because they do not consider higher order partial waves for which this experiment is sensitive.

If we consider only s and p waves in the final state, the allowed transitions and their angular distributions are the following:

Transition amplitude	Angular distribution
$a = ({}^3P_1 \rightarrow {}^3S_1)$	Isotropic
$b = ({}^1S_0 \rightarrow {}^3P_0)$	Isotropic
$c = ({}^1D_2 \rightarrow {}^3P_2)$	$1/3 + \cos^2\theta$

All models predict that c is the dominant amplitude. This agrees with most experiments; the angular distributions are roughly $0.25 + \cos^2\theta$ within a 6% to 20% experimental error. Furthermore, in transition c the pion angular momentum is parallel to both nucleon spins and allows an intermediate πN (3/2,3/2) resonant state corresponding to the N*(1236) resonance. The N* resonance would be manifested in a peak at 600 Mev incident neutron energy in the total cross section. Experiments confirm a strong peak in that region.

Shiff et al. consider higher order partial waves. The important waves are those that interfere with the dominant transition ${}^1D_2 \rightarrow {}^3P_2$. These transitions are:

$$d = ({}^3F_2 \rightarrow {}^1D_2)$$

$$e = ({}^3F_4 \rightarrow {}^1G_4) \quad .$$

The results of their analysis show that a and d are negligible, and $b \simeq e \simeq c/10$. They find that a fourth power $\cos\theta$ term is important and is the same order of magnitude as the $\cos^2\theta$ term. A comparison of our results with this theory will be given in Section IV.

II. EXPERIMENTAL APPARATUS

II-A. General Description

A floor plan of the experiment is shown in Figure 1. A beryllium target 4.0 inches long and 0.5 inch square was put inside the cyclotron at a radius of 172 inches as an "internal target" to create neutrons. The neutrons that came off at approximately zero degrees with respect to the bombarding protons passed through steel collimators 2.0 inches in diameter and totaling 14 feet in length. Charged particles formed in the internal target were swept away from the collimator by the magnetic field of the cyclotron. Most of the gamma rays produced were eliminated by a lead γ converter 2 inches thick.

Charged particles created in the collimator were eliminated by a sweeping magnet farther downstream. The neutrons passed through a liquid hydrogen target and then through beam monitor counters.

The deuterons were detected by a coincidence between counters D1 and D2. The time delay of the pulses from D1 and D2 was carefully adjusted to accept deuterons. and reject the faster moving protons. The orbits were recorded by using four spark chambers C1 through C4, and reading out the spark locations with a magnetostrictive readout system. Between C2 and C3 was an analyzing magnet on a swivel mount and tracks so that its position would easily be changed.

An on-line PDP-5 computer and magnetic tape unit was used to continuously monitor the experiment and record the digitized spark coordinate readings, beam monitor counters, and time of flight between D1 and D2.

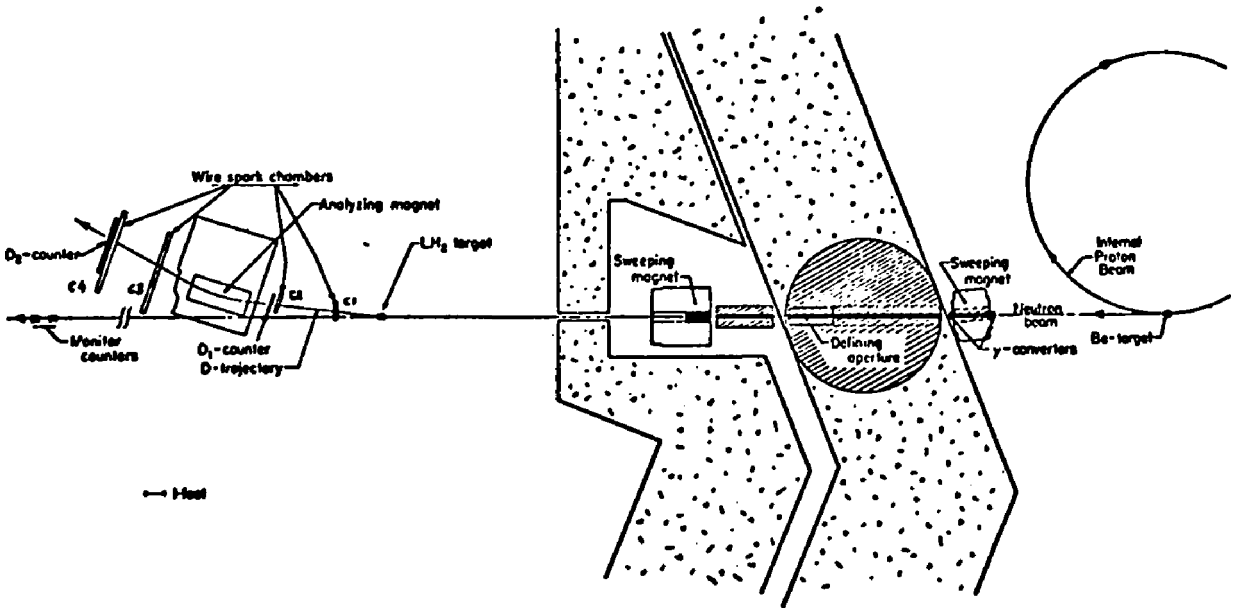


Figure 1: Floor Plan

II-B. Neutron Beam

The energy distribution of neutrons created in a beryllium target bombarded by protons has been measured by a Dubna group[10] that used a cyclotron operating under conditions similar to our experiment except that the cyclotron energy was 680 Mev instead of 720 Mev. Their neutron energy distribution was scaled by 720/680 to estimate our distribution. The distribution which we used came from the γd experiment. It was obtained by assuming detailed balance and using the total cross sections measured in γ+d → n+p experiments. The number of γd events in a particular energy range (after accounting for efficiencies) was divided by the total cross section to obtain the relative number of neutrons. This neutron distribution is compared to that obtained by the Russian experiment in Figure 2. The general features of these two distributions are the same.

There are large uncertainties in the total cross section measurements in the γ+d → n+p experiments. This will result in an equally large uncertainty in the neutron energy distribution. Further details are given in Section IV-D.

The spatial distribution of neutrons in the beam was found by projecting the deuteron orbit from chambers C1 and C2 back to the target midplane to find the interaction point in the target. The distribution of the target interaction points should be the same as the spatial distribution of the neutron beam for a target of uniform thickness. The measured distribution is shown in Figure 3. It is slightly smeared by the finite target length and Coulomb scattering of the deuteron.

The neutron beam intensity was continually monitored by three identical sets of three counters for reliability and redundancy. The first in each set was an anti-counter which made sure the second two counters were not counting charged particles in the beam. A polyethylene block after the first counter created charged particles which the second and third

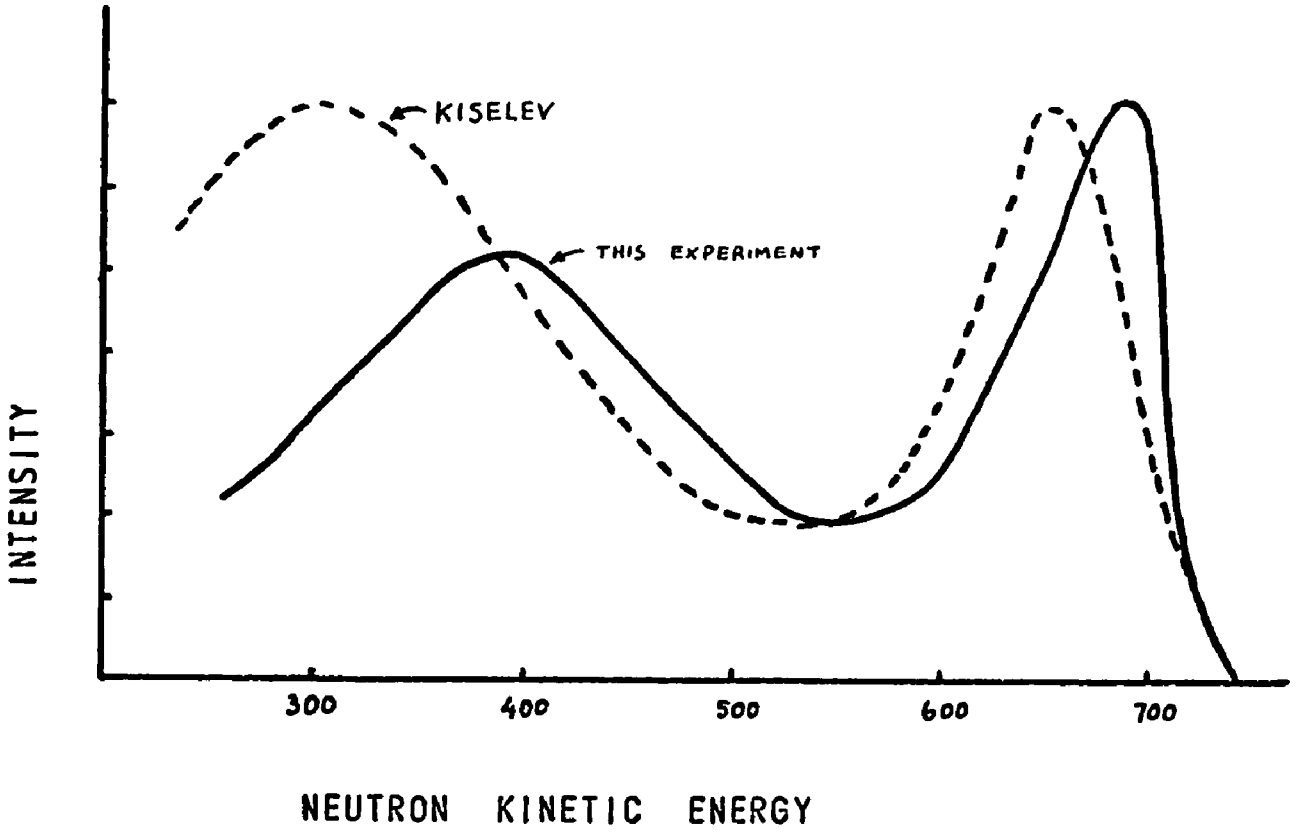


Figure 2: Neutron Energy Distribution

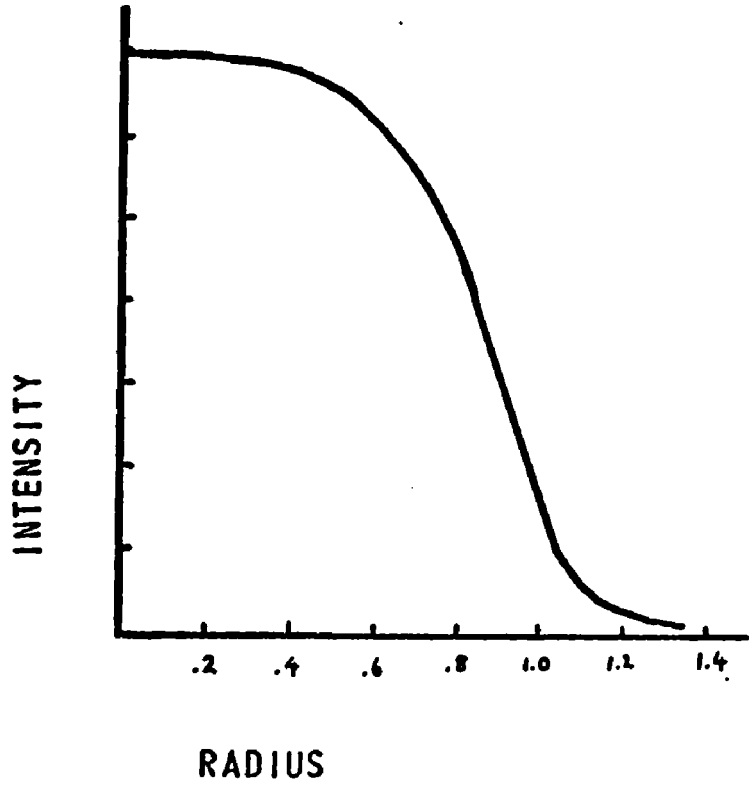


Figure 3: Beam Profile

counters detected in coincidence. The three sets of counters tracked to within 1% of each other during the experiment.

II-C. Hydrogen Target

The liquid hydrogen was contained in an aluminum cylinder 7.5 cm in diameter with 4 mil mylar end caps. A drawing of the target is shown in Figure 4. A reservoir above the target kept it filled with hydrogen. An extra line ran from the bottom of the target to a valve and then a vent. Ordinarily the valve was kept open so that boiling hydrogen in the line was vented. But, for a target empty run, the valve was closed so that the vapor pressure of the boiling hydrogen forced the liquid out of the target and into the reservoir. The target was surrounded by a vacuum jacket with mylar windows to allow the neutron beam to pass through and the deuterons to exit.

The material in the beam was minimized to reduce interactions in the target walls and Coulomb scattering. There was 0.44 gm/cm^2 of hydrogen in the target. The target walls consisted of 0.05 gm/cm^2 of mylar and 0.03 gm/cm^2 of aluminum.

II-D. Magnetostrictive Readout System

A number of methods to record the locations of a spark in a spark chamber have been devised which avoid the slow and tedious analysis of photographic film.[11] The method used in this experiment took advantage of the properties of a magnetostrictive (MS) delay line to digitize the spark coordinates. The two planes of each spark gap were made out of closely spaced fine wire, rather than a foil. The wires were connected to a bus bar at one end and were open at the other, as shown in Figure 5. One plane was grounded. When a particle was detected, the other plane was pulsed with a high voltage so that a spark was formed and current flowed only in those wires through which the spark passed. Two fiducial wires located outside the active volume (one at each end of the MS

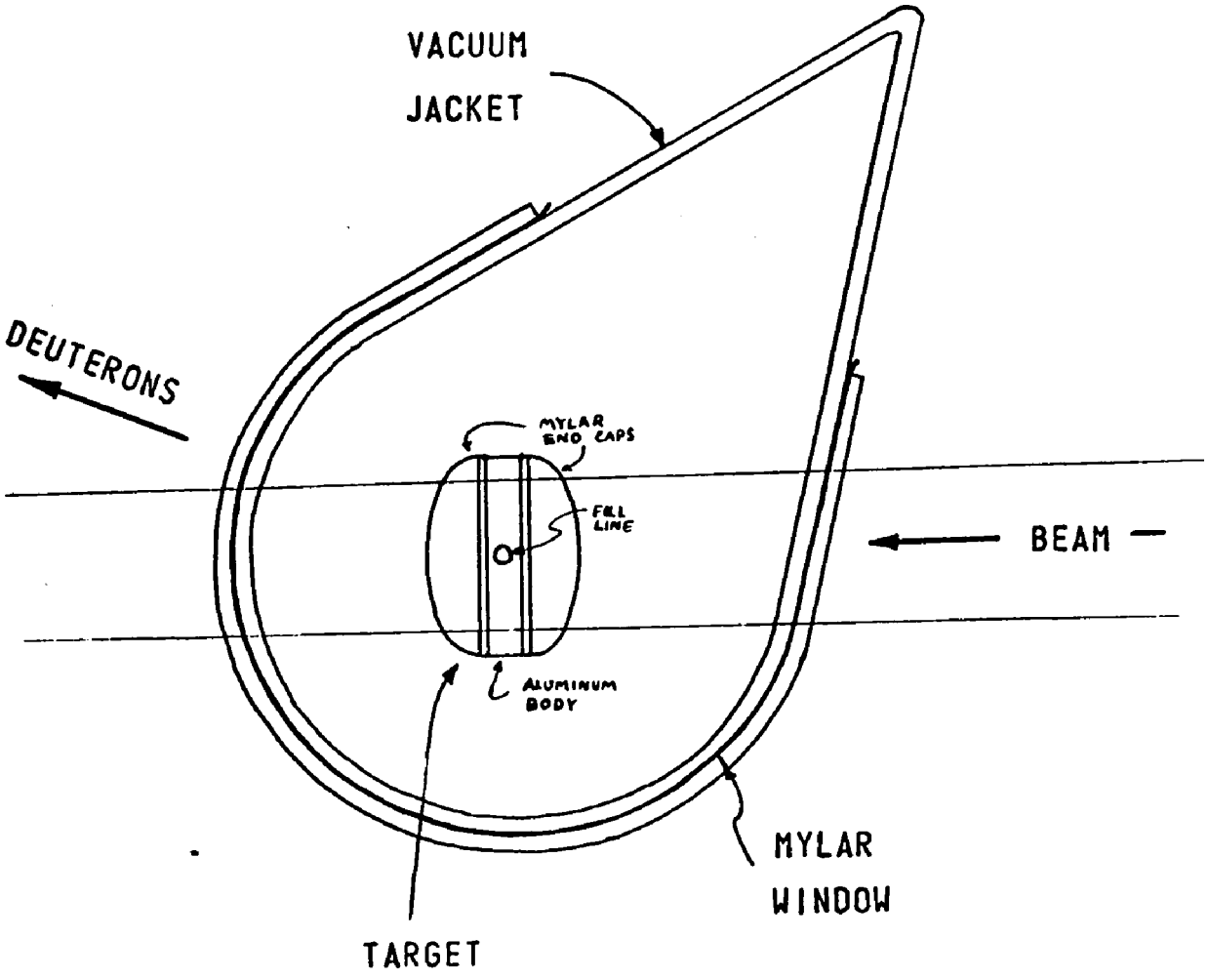


Figure 4: Target

wire) were pulsed along with the high voltage. The fiducials were accurately placed and acted as a calibration of the readout system. The dotted lines in Fig. 5 show the flow of current through the chamber wire. A detailed account of a MS readout system is given in Reference 12.

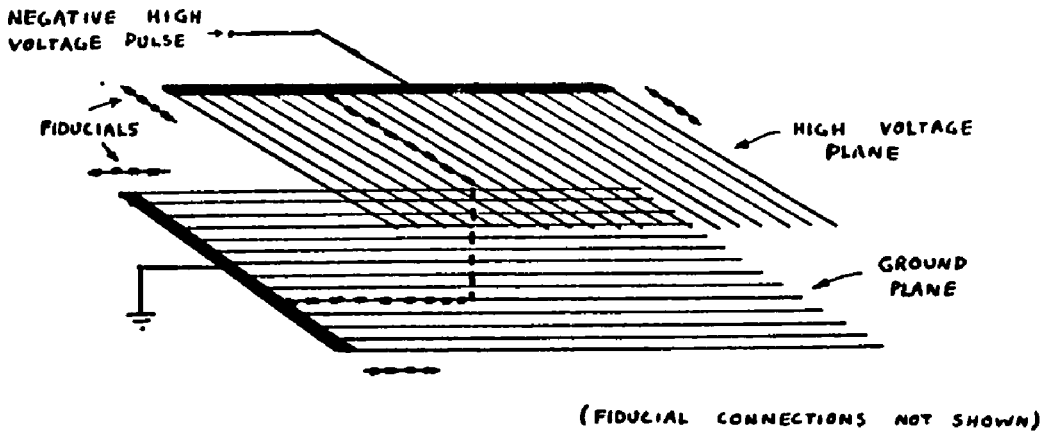
A magnetostrictive wire 7 mils in diameter was placed in close proximity to the wires near the bus bar and perpendicular to the wires. Figure 6 is a view of the MS line looking at the ends of the wires in one plane of the spark chamber. The magnetic fields of the wire which was sparked and the two fiducials cause a local magnetostrictive deformation in the MS wire. The strain in the wire as a function of distance is shown in Figure 7. The deformation travels at the speed of sound to the ends of the MS wire where they are damped. Near one end of the MS wire is a pickup coil connected to a preamplifier. The coil puts out a signal of about 30 Mv which is amplified to 1.5 volts. For further details of the MS wire, pickup coil, and amplifier, see Ref. 12.

The first signal to arrive at the pickup coil comes from the "start fiducial". This signal gates on a 20 MHz pulser which is counted by two scalers. The second signal comes from the sparked wire, and it gates off one of the scalers. The third signal is the "stop fiducial" (or possibly a second spark). It gates off the second scaler. If there is just one spark in the chamber, the distance, D, from the sparked wire to the start fiducial is given by the relation

$$D = F \times \frac{\text{first scaler reading}}{\text{second scaler reading}}$$

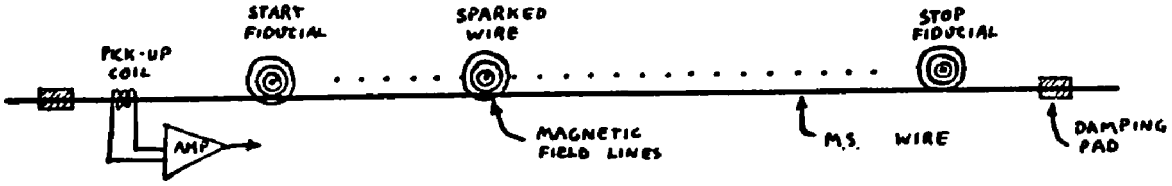
where F is the distance between the start and stop fiducial.

For four chambers, each with four planes, and two scalers for each plane, there is a total of 32 scaler readings. These were stored in the PDP-5 computer memory and read onto tape after every 12 events.



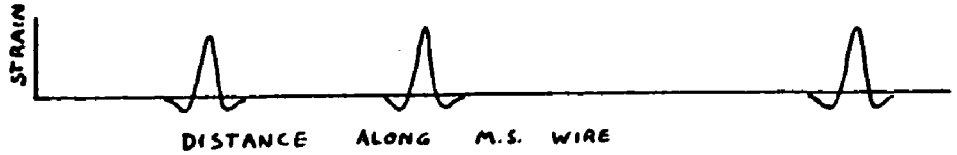
WIRE CHAMBER SCHEMATIC

Figure 5



MAGNETOSTRICTIVE DELAY LINE

Figure 6



M.S. WIRE STRAIN

Figure 7

II-E. Spark Chamber Construction and Performance

Chambers C3 and C4 were built by LRL[13]. They were constructed of 6 mil aluminum wires spaced 1 mm apart and glued to an epoxy-fiberglass frame. (See Figure 8.) Each chamber had two gaps and four wire planes. The first plane had vertical wires, and the last plane had horizontal wires. These planes were grounded. The second and third planes had wires which were 45° with respect to the ground planes and perpendicular to each other. These planes were pulsed at high voltage. Slots were milled in the frames so that a magnetostrictive wire mounted on an aluminum bar could be slid in to sense the location of the spark. The first and last wires of each plane were connected to the high voltage through a resistor and inductor in series so that they would draw current every time the chamber was pulsed, and thus they furnished start and stop fiducials for the read-out electronics.

Chambers C1 and C2 were constructed at the University of Michigan. The frames were made of lucite and the "wires" were 20 mil by 1 mil aluminum ribbons on a sheet of mylar 2 mils thick. Printed circuit techniques were used to etch the grid of wires out of aluminized mylar. The planes were then glued to the lucite frames in a manner similar to optical chamber construction. Each of these chambers had four gaps: four wire planes at ground potential, and two aluminum foil planes pulsed at the high voltage. The construction is shown in Figure 9. Slots were milled in the frames for the MS sensors.

After the planes were glued to the frames, fiducial wires were soldered accurately in place. All the fiducials of a chamber were wired in series and pulsed from a common source.

The chambers were pulsed by a triggered spark gap designed and constructed at LRL[14]. The high voltage plane of each gap was fed by separate capacitor-resistor combina-

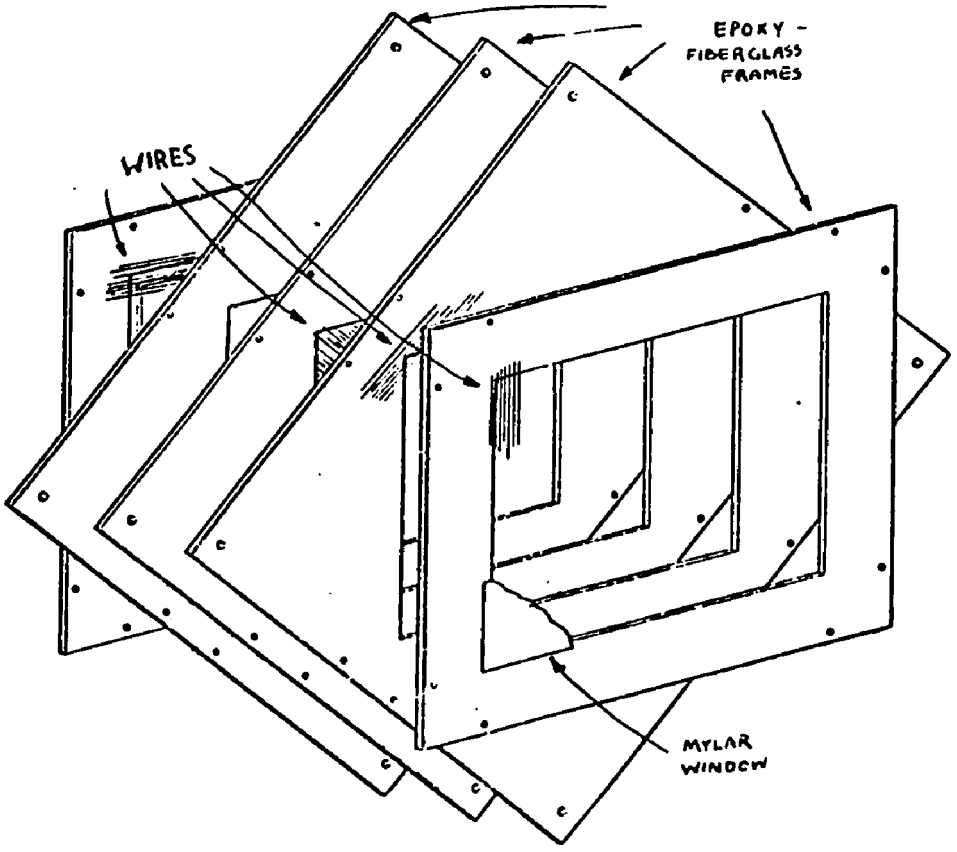
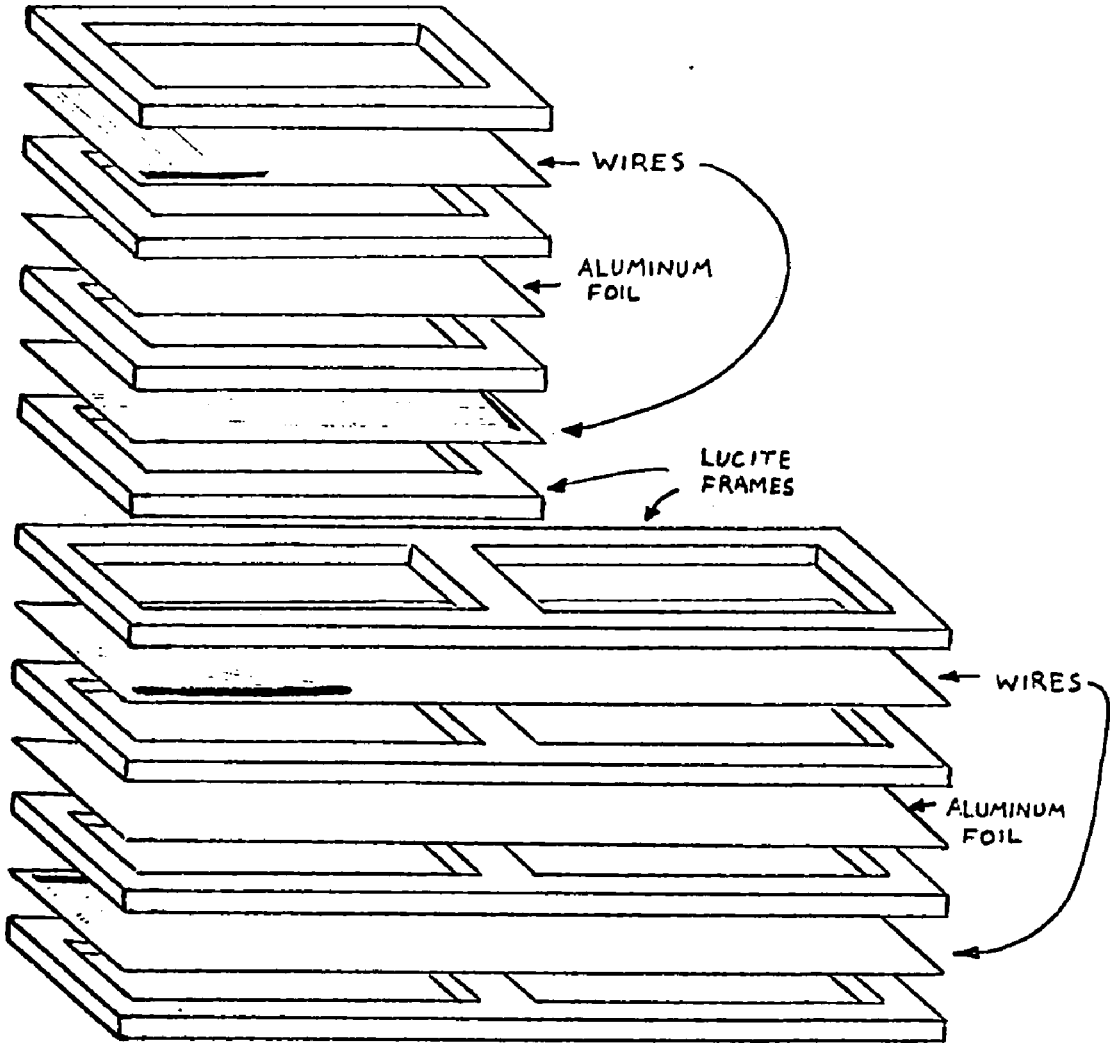
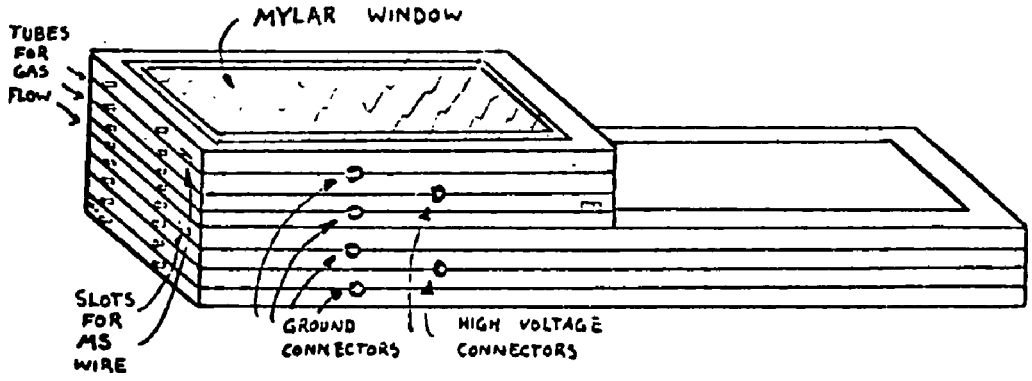


Figure 8: Chambers 3 and 4



EXPLODED VIEW



COMPLETED CHAMBER

Figure 9: Chambers 1 and 2

tions which were adjusted to give a uniform performance of high efficiency (about 98%) and large MS signals. Each gap had a constant 50 volt clearing field to sweep away ions from unrelated events and reduce the recovery time.

Table 1 shows the number of events for a typical run vs. the number of sparks found in the sixteen gaps. Notice that about half the events have one spark for each gap.

Table 1

Number of Events vs. Number of Sparks

29	events with less than	12	sparks
30	events with	12	"
88	" "	13	"
291	" "	14	"
1014	" "	15	"
1725	" "	16	"
600	" "	17	"
182	" "	18	"
48	" "	19	"
11	events with more than	19	"
4018	total events		

II-F. Spectrometer

Chamber C1 was mounted so that it was stationary with respect to the target. C2, C3, and C4 were mounted stationary with respect to the magnet. The momentum analyzing magnet was a forty ton C magnet with a rectangular pole face 36 by 16 inches and a gap 8 inches wide. The LRL magnet group measured the vertical component of the field at 5151 different points in a lattice of 79x29x3 points in the X, Y, and Z directions respectively. These measurements were made for

six different currents ranging from 980 to 2000 amps, giving central fields which range from 10450 to 17550 Gauss.

Deuterons from π°d production come from the target at angles from 0° to 14° and with momenta from 675 to 1500 Mev/c. In order to span the deuteron angles and momenta of interest, 9 magnet settings with different currents and positions had to be used. The magnet was moved to three positions in order to cover the angular region. The first position covers angles from 0° to 6.5°. The second covers 5.25° to 10.0°; and the third covers 8.0° to 14.0°. For each of these positions, different current settings were used to cover the momentum space. Figure 10 is a diagram of the laboratory phase space. The cross hatched areas show the region covered by each of the magnet settings. The heavy curves show the allowed kinematic regions for π°+d production for incident neutron energies between 285 and 700 MeV.

II-G. Counters

Aside from the beam monitor counters, only three other counters were used in this experiment. They were constructed of Pilot B plastic scintillator, and were located as shown in Fig. 1. D1 had dimensions 8 x 10 x 1/16 inches. A1 was 8 x 5 x 1/4 inches and was used in anticoincidence. Its function was to effectively reduce the size of D1 to limit the angular acceptance of deuterons. If was located in front of D1. D2 was 12 x 22 x 1/4 inches. These counters were coupled to 56AVP photomultiplier tubes using lucite light pipes.

II-H. Electronic Logic

D1, D2, and A1 were connected to Chronetics discriminator modules[15], and then to an AND gate with D1 and D2 set for coincidence and A1 set for anticoincidence. Pulses

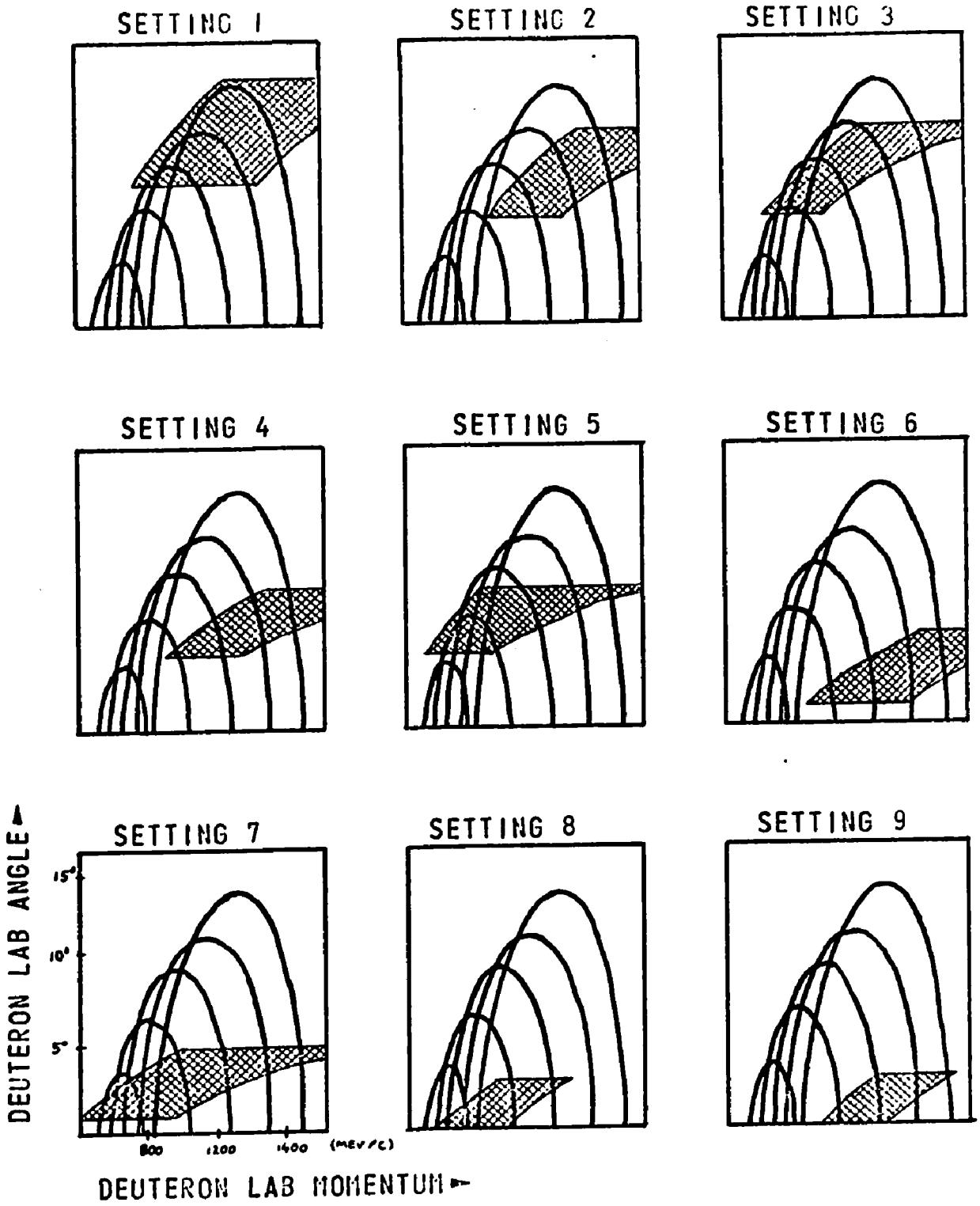


Figure 10: Deuteron Phase Space Covered by Spectrometer

from D1 and D2 were also sent to a module which digitized the time difference to an accuracy of ± 1/2 nsec. The output of the AND gate triggered the spark chambers, enabled the MS readout electronics, and started a 200 msec long gate which turned off the whole system so that the spark chambers would recover. Data taking rates were typically four events per second.

III. DATA ANALYSIS

III-A. Location of Sparks

In locating the path of a particle through a four gap spark chamber, we find a redundancy of information coming from the four wire planes oriented in four different directions. This redundancy was used to remove ambiguities in multispark events and to improve efficiency and accuarcy. The information was handled in a very efficient way using a series of subroutines developed by LRL programmers[16].

Initially it was assumed that the distance between the four planes in a chamber is zero, so that the problem reduced to that of finding the intersection of an orbit in one plane rather than the more complicated problem of finding an orbit through four planes. For each event there could be zero, one, or two spark locations recorded in each plane. The first program tried all possible combinations using one wire from each plane. For each combination it calculated a point P=(X,Y), and its "residual" r which is a measure of its goodness of fit.

P and r were determined in the following way: Each wire has the equation

$$A_i X + B_i Y = C_i \quad , \; i=1,4 \tag{3}$$

where A_i and B_i are the direction cosines of each of the four wires. In matrix notation Equation 3 becomes

$$\mathbb{M}\,\mathbb{P} = \mathbb{C} \tag{4}$$

$$\text{where } \mathbb{M} = \begin{pmatrix} A_1 & B_1 \\ A_2 & B_2 \\ A_3 & B_3 \\ A_4 & B_4 \end{pmatrix}, \quad \mathbb{P} = \begin{pmatrix} x \\ y \end{pmatrix}, \quad \text{and} \quad \mathbb{C} = \begin{pmatrix} C_1 \\ C_2 \\ C_3 \\ C_4 \end{pmatrix}.$$

However, in solving for P this system is overdetermined and has no solution in general. Equation 4 can be modified:

$$\mathbb{M}\,\mathbb{P} - \mathbb{C} = r \quad , \quad \text{where } r = \begin{pmatrix} r_1 \\ r_2 \\ r_3 \\ r_4 \end{pmatrix} . \qquad (5)$$

There exists a unique solution of Equation 5 which minimizes the sum of the squares of the residuals r_i. The solution can be written as

$$\mathbb{P} = \mathbb{M}^I \, \mathbb{C}$$

where $\mathbb{M}^I$ is the generalized inverse of $\mathbb{M}$. This equation and solution are discussed by Rust et al[17].

The residuals r_i turn out to be the perpendicular distance from point P to the wire in plane i. If the residuals were small enough (less than 1/2 inch) the corresponding wires were used in determining the orbit. If the residuals were too large, the whole program was repeated using all possible combinations of wires from each of three planes. If an acceptable solution still did not exist, two planes were used (in chamber 1). However, two-plane solutions were usually rejected for other reasons, e.g. none of the other chambers fired. In this experiment chamber one had the largest number of two wire events. It was found that almost all of these events were protons which were created or deflected in the frame of chamber one and thus did not pass through it.

After the proper set of wire combinations was found for the four chambers, the particle orbit was calculated. The orbit was found for the particle before it entered the magnet from chambers 1 and 2, and after it left the magnet from chambers 3 and 4. The orbit was taken to be the straight line which minimized the sum of the squares of the perpendicular distances to each of the 8 wires in the first or second

pair of chambers. The solution involves solving linear equations and is straightforward[18]. The calculated orbit is given in terms of five parameters: three coordinates which designate a point through which the orbit passes, and two slopes which give the directions of the orbits.

III-B. Alignment Checks

To insure the accuracy of the spatial reconstruction of the experiment, we measured and compensated for errors in the alignment of the fiducial wires in each gap of each chamber. This was easily done with a special program and a batch of raw data.

The nominal locations of the fiducials were used to check each event through chambers 1 and 2. Those particles whose orbits were perpendicular (within 0.5 degrees) to the chambers were used to calculate the residuals. For these perpendicular orbits the average of the residuals over a large number of events should be zero if the alignment of the fiducials was correctly done. If the average residual for a particular gap was displaced from zero, the location of the fiducial could be adjusted to compensate for this.

On the basis of this analysis, a few fiducials needed adjustments from 0.2 to 0.75 mm. After adjustments the program was run again to insure that the residuals were zero. This same procedure was repeated for chambers 3 and 4.

The accuracy of the surveyed positions of the four chambers in the spectrometer was checked by collecting data with the magnet turned off. Particles would then go straight through all chambers without bending. The measured spark locations in the chambers should be collinear if the surveying were done accurately. The deviations were found to vary from 0.0 to 1.3 mm for the various positions. After these corrections were added, the programs were run again to verify

the collinearity of the orbits.

III-C. Momentum Determination

After the orbits of the particle (before entering and after leaving the magnet) were calculated, the momentum of the particle was found from the amount of bending in the magnet. The momentum could not be calculated directly but had to be found by successive approximations.

The first step was to find an approximate momentum P using the formula

$$P_1 = \frac{2\ q\ B\ L}{\sin\alpha_{in} + \sin\alpha_{out}} \times \text{correction.} \qquad (6)$$

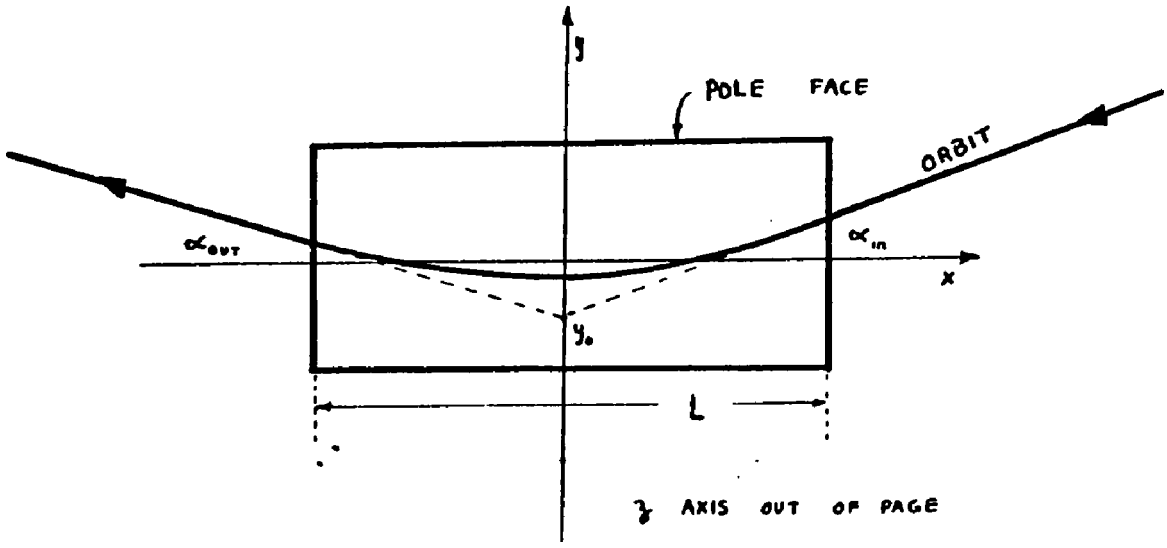
This formula is exact for a particle of charge q traversing a uniform field B in a rectangular region of length L. α_{in} is the incoming angle and α_{out} is the outgoing angle. (See Figure 11.) The correction is a polynomial with 81 parameters, c_{ijkl}:

$$\text{correction} = \sum_{i=1}^{3}\sum_{j=1}^{3}\sum_{k=1}^{3}\sum_{l=1}^{3} c_{ijkl}\, s_i^{i-1} s_o^{j-1} y_o^{k-1} z_o^{l-1}$$

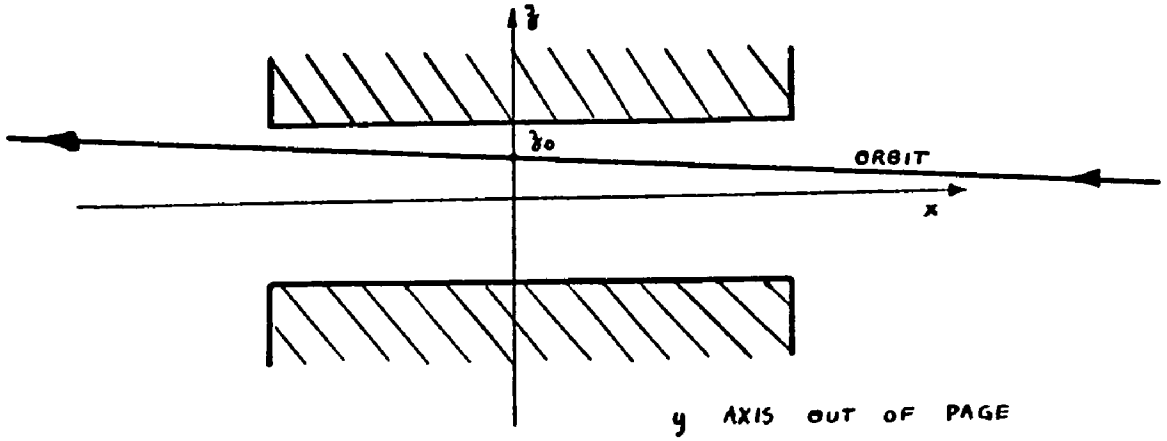
where s_i = slope of incoming orbit
s_o = slope of outgoing orbit
y_o = zero intercept of orbit on y-axis (Fig. 11)
z_o = zero intercept of orbit on z-axis.

The 81 parameters were found by generating several hundred orbits of known p, applying Equation 6 to each orbit, and adjusting c_{ijkl} to minimize the total RMS error.

Next a more accurate numerical intergration was done. The approximate solution for momentum P_1 was used in tracing the path of the particle through the magnetic field step by step; the orbit was bent at each step according to the



TOP VIEW



SIDE VIEW

Figure 11: Geometry of Orbits

direction and magnitude of the field. The value of the field at each point was interpolated from a lattice of 5151 field measurements. After the calculated orbit was clear of the field, its intersection through the next spark chamber was computed. If this intersection point was within 0.5 mm of the actual spark location, the calculation was close enough and P is within 0.2% accuracy. If the intersection point was further than 0.5 mm, a second approximation was made. Eq. 6 was used again; this time $\sin\alpha_{out}$ was determined from the integration intersection point rather than the actual spark location. This value for P (P_2) gave a quantitative estimate of the accuracy of Eq. 6. A new trial momentum P_{new} was obtained from

$$P_2 = P_1 + (P_1 - P_{new}).$$

This new value of P was used, and another integration was done to check it. In almost all cases no more than two integrations were needed to obtain the desired accuracy. The average computer time per event was 0.2 sec at the LRL 6600 computer.

In the orbit integration process only three chambers were needed: two were used to find the incoming orbit, and one was used to check the intersection point of the outgoing orbit. This was useful if one of the chambers did not fire. Also, the unused chambers were used as a final systematic check of the accuracy of the spectrometer in the following manner: The computed orbit was projected to the unused chamber and the deviation from the chambers actual spark location was plotted in a histogram. These distributions had displacements ranging from -0.6 to 1.8 mm for the nine magnet positions. The resulting systematic errors are discussed in Section IV-B. The width at half maximum ran from 5 to 6 mm. This corresponds to a spread in the momentum measurement of approximately 2.0%. It agrees with the spread in momentum caused by multiple Coulomb scattering in the spectrometer.

III-D. Solid Angle Calculation

The number of deuterons detected is proportional to the solid angle subtended by the detecting apparatus. The solid angle differential is

$$d\Omega = \sin\theta \, d\theta \, d\phi$$

where θ and ϕ are the polar and azimuthal angles.

The solid angle for a particle leaving the origin of the coordinate system with its polar angle in the range $(\theta-\frac{\Delta\theta}{2})<\theta'<(\theta+\frac{\Delta\theta}{2})$ and its azimuthal angle having the limits ϕ_L and ϕ_U is given by

$$\Delta\Omega = \int_{\phi_L}^{\phi_U} \int_{\theta-\frac{\Delta\theta}{2}}^{\theta+\frac{\Delta\theta}{2}} \sin\theta' \, d\theta' \, d\phi'$$

$$\approx \sin\theta \, \Delta\theta \, (\phi_U-\phi_L)$$

for $\Delta\theta$ small. The limits ϕ_U and ϕ_L were determined by the edges of counters D1 and D2 and by the pole faces of the magnet. The limits of ϕ through D2 depend on the bending through the magnet, and is therefore related to the momentum. Thus ϕ_U and ϕ_L are functions of θ and P:

$$\Delta\Omega(\theta,P) = \sin\theta \, \Delta\theta \, [\phi_U(\theta,P)-\phi_L(\theta,P)].$$

Because of vertical symmetry of the spectrometer, $\phi_U=-\phi_L$. Thus,

$$\Delta\Omega(\theta,P) = 2\sin\theta \, \Delta\theta \, \phi_U(\theta,P).$$

For a finite sized target, the deuteron does not necessarily leave from the origin; it can be formed anywhere the beam hits the target. In this case, ϕ_U is also a function of the location of the target interaction point: $\phi_U = \phi_U(\theta,P,x,y,z)$. To obtain the solid angle, ϕ_U must be weighted according to the neutron intensity distribution at the interaction point, and integrated over the volume of

the target:

$$\Delta\Omega(\theta,P) = 2 \sin\theta \, \Delta\theta \iiint \phi_U(\theta,P,x,y,z) \; I(x,y) \; dx \, dy \, dz$$

where x,y, and z are coordinates in the target and I(x,y) is the normalized spatial neutron energy distribution.

This type of calculation is usually done with a Monte Carlo program, but in this case, rather than spanning the variables randomly, it was found that the variables could be spanned uniformly in small steps without using too much computer time. This is equivalent to a numerical integration.

Since the deuteron in the lab system has a maximum angle of only 14°, ϕ_U will have very little z dependence. For this reason the target was considered to be a two dimensional disc in the x-y plane. To perform the integration, the target was divided into 2.5 mm squares (approximately 530 squares for a radius of 3.3 cm) in the x-y plane, and the relative neutron flux was calculated for each square. To find $\Delta\Omega(\theta,P)$, a particular θ and P were chosen. For each target square ϕ was varied in 0.1° steps until an integration boundary was reached. Written as a numerical integral, the solid angle becomes:

$$\Delta\Omega(\theta,P) = 2 \sin\theta \, \Delta\theta \sum_{\text{target}} I(x,y) \; \phi_U(\theta,P,x,y).$$

For each step of ϕ the point of intersection with D1 was found from simple geometry and the point of intersection with the pole face was found from Eq. 6. In this case P is known and $\sin\alpha_{out}$ is unknown. From Eq. 6 the solution for $\sin\alpha_{out}$ is:

$$\sin\alpha_{out} = \left(\frac{2qBL}{p} - \sin\alpha_{in}\right) \times \text{correction} \qquad (7)$$

The correction involves a different set of 81 parameters multiplied by various powers of P, $\tan\theta$, and the target point.

If the neutron distribution is normalized so that

$\sum_{target} I(x,y) = 1$, the sum $2 \sum_{target} I(x,y)\phi_U$ is a weighted average of ϕ_U. It is easy to compare this with what would be expected and thus check the reasonability of the calculation. Let

$$\bar{\phi}(\theta,P) = 2 \times \sum_{target} I(x,y)\ \phi_U(\theta,P,x,y)$$

so that the solid angle can be written as

$$\Delta\Omega(\theta,P) = \sin\theta\ \Delta\theta\ \bar{\phi}.$$

For consistency in the data analysis, the same criteria used in the integration were used to reject events: if an event fell outside the integration boundaries ("fiducial volume"), according to Eq. 7, the event was rejected. The fiducial volume was made to be smaller than that determined by the counters and pole faces - small enough so that no events were lost through Coulomb scattering or through an inaccuracy in Eq. 7. In the course of the data analysis, histograms and scatter plots were made which compared computed orbits with actual orbits to make sure the fiducial volume was small enough, but no smaller than necessary.

III-E. Data Processing and Binning

In the first step of the data reduction, the raw data tape from the PDP-5 on-line computer was processed on the LRL Control Data 6600 computer. The fiducial drift was constantly checked and accounted for event by event. The magnetostrictive scaler readings were translated into spatial dimensions. The spark locations and orbits were found and the orbit integrations through the magnet performed to get the momentum. The orbits, momenta, time of flight, monitor counters, etc., of the half million events were recorded on fifty "reduced data tapes".

Next, the reduced data tapes were run to set and check

the fiducial volume. The orbits were projected back to the target to check the size, location, and intensity distribution of the beam. With this information the correction parameters for the solid angle program were generated. The reduced data tapes were run again; the parameters of the good events which fell inside the fiducial volume were stored in histograms (bins). The mortality rate for those events which were rejected are tabulated for a typical run in Table 2.

Table 2
Mortality Rate of Events

	All Chambers	Missing Chambers 1	2	3	4
Good events	7030	1	5	44	12
Hit pole face	845	0	0	2	1
θ_L too large	26	0	0	1	0
θ_L too small	282	0	0	0	0
P_L too large	67	0	0	1	0
P_L too small	1049	0	1	9	66
Outside target	1121	160	0	2	0
Misc. rejects	39	0	0	0	1

It would be desirable to bin the events in two dimensions according to the laboratory polar angle and momentum of the outgoing deuterons. Since there is a heavy contamination of protons, the time of flight (TOF) information might be used to obtain the velocity of the particle. The momentum and velocity would then give the mass according to the formula, $P=(m_0/\sqrt{1-v^2/c^2})v$. For low momentum particles it is possible to distinguish the mass of a deuteron from a proton, but the timing resolution of ±1 nsec makes it impossible to completely resolve high momentum particles. Figure 12 shows typical

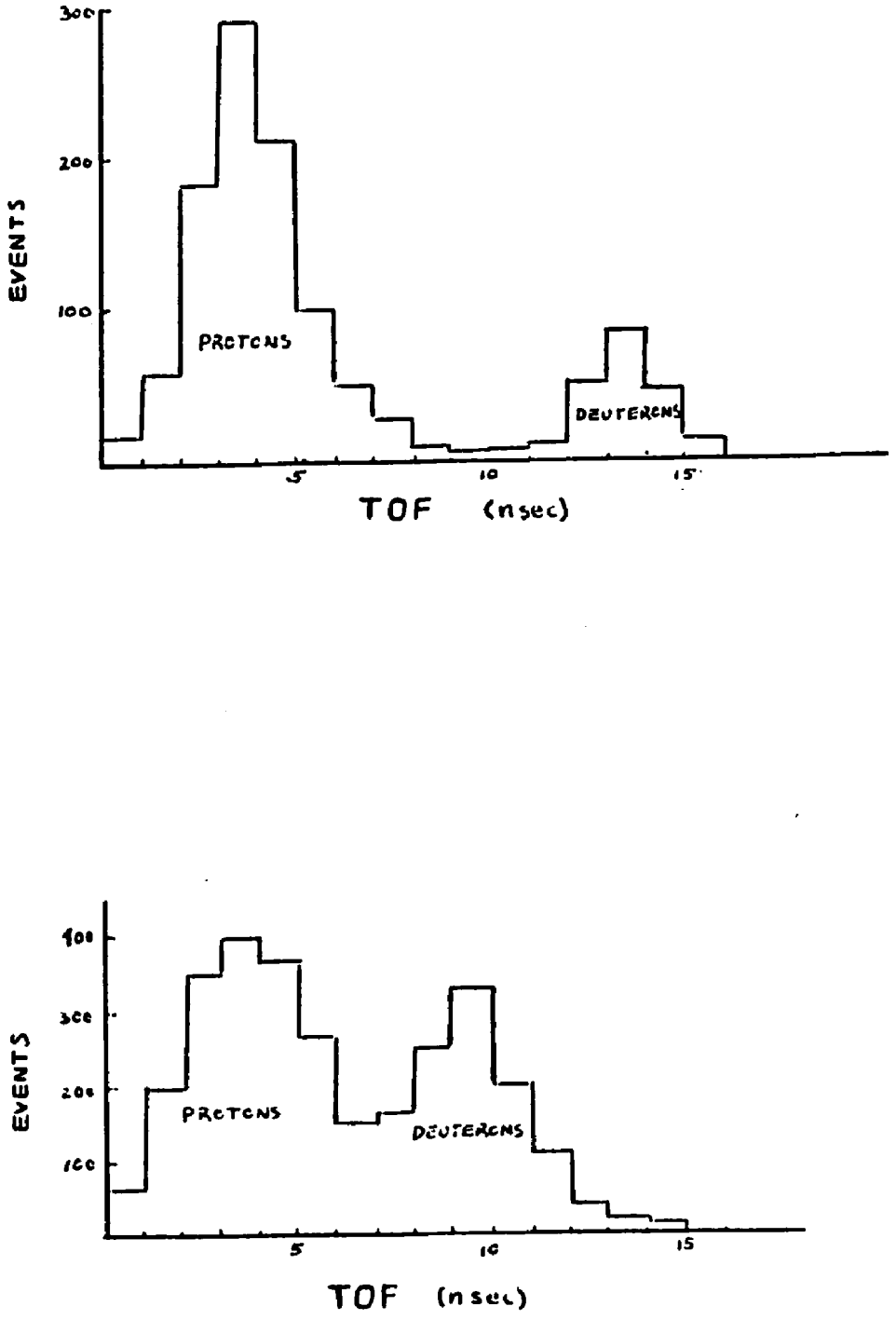


Figure 12: Typical Histograms for the Time of Flight

histograms for a case with relatively good and relatively poor separation. Therefore a single event can not always be unambiguously determined to be a proton or a deuteron.

The only alternative is to bin the events in three dimensions according to angle, momentum, and time of flight. After all the data are binned, it is possible to separate the protons and deuterons on a statistical basis. The shapes of the histograms in all cases were found to fit two separated gaussian functions to a high degree of accuracy. Thus, gaussian shapes were fitted to the data, and the area of each gaussian respectively gave the number of protons and deuterons for that bin. The bin sizes are as follows: 26 angle bins 1/4° wide, 45 momentum bins 20 Mev wide, and 30 TOF bins 1 nsec wide. This makes a total of 35100 bins. Word packing techniques had to be used to fit this into the computer memory and still leave room for the rest of the program. This procedure is described in detail in the next section.

The binned data from each of the fifty data tapes were punched on cards. The cards were totaled so that all the data were on nine separate decks of cards corresponding to the nine magnet positions. The same procedure was followed for the target empty runs.

It was found that typically 3.5% of the triggers did not have enough sparks to determine the orbits. These were mostly accidental triggers or stray particles which did not pass through some of the chambers.

III-F. Separation of Protons and Deuterons

The separation of protons and deuterons entails a rather involved procedure using the method of maximum likelihood. In summary the separation proceeded as follows:

1. An abbreviated form of the 35,100 bins was printed out.

2. A representative sample of angle and momentum bins were chosen. For each of these bins the time of flight histogram was plotted. The locations of the peaks of the deuteron gaussians were measured by eye to within 0.2 nsec accuracy to give a first approximation.

3. A function with seven parameters was fitted to this sample to give the gaussian peak location as a function of angle and momentum.

4. The average deuteron gaussian width was measured. (It is fairly independent of angle and momentum.)

5. A polynomial with four parameters was added as a correction to the function in step 3. It has the form $C = a_1+a_2\theta+a_3P+a_4P\theta$, where θ and P are the angle and momentum.

6. A polynomial with four parameters was added as a correction to the average width in step 4. It has the same form: $C' = b_1+b_2\theta+b_3P+b_4P\theta$.

7. The location of the proton gaussian (as a function of deuteron width and location) could be found exactly using maximum likelihood; and its width could be found using a very good approximation.

8. The eight parameters a_i and b_i were adjusted to maximize the likelihood of the fit of the data using the method of steepest ascent. For this fit the number of deuterons were calculated for each bin.

9. An eight dimensional ellipsoid was computed in the a_i, b_i space such that the probability is one half maximum on its surface. For each angle-momentum bin this ellipsoid was projected onto the two dimensional subspace: width vs. location of the gaussian. The projection is an ellipse.

10. For each point on this second ellipse, the number of corresponding deuterons could be computed. The maximum and minimum give the separation error.

This procedure allows the gaussian parameters (width and location) to vary until the most likely fit is found, with the constraint that the variation be smooth from bin to bin.

In two of the magnet positions (one with poor separation and one with good separation) it was found that the proton-deuteron separation error was about 1% of the statistical error. Therefore steps 9 and 10 were dropped for the remaining seven positions.

Table 3 shows the disposition of the events for the nine magnet positions. The table shows the numbers of deuterons remaining after fiducial cuts were applied and protons eliminated.

Table 3
Disposition of Events (in thousands)

Magnet Position	Total Triggers	Fiducial Cut	Protons Eliminated
1	198	124	50
2	16	6	3
3	12	6	3
4	36	27	11
5	44	19	12
6	38	20	17
7	40	24	9
8	50	5	3
9	48	5	3
Total	482	266	111

III-G. Corrections to Data

After the deuterons were separated from the protons, other corrections were applied. These are energy loss and

Coulomb scattering of the deuteron in passing through the target and spectrometer, contamination from the reaction $n+p \rightarrow \gamma+d$, events originating in the walls of the target, and absorption of deuterons.

Energy Loss

The energy loss as a function of deuteron momentum was calculated using a LRL program[19]. The thicknesses of the various absorbing materials were put into the program. The mean energy loss and energy loss distribution were calculated using Bethe's stopping power formula[20]. The width of the distribution was found to be much smaller than the resolution of the spectrometer, and therefore was neglected. The result of the energy loss correction is a small addition of momentum to the value measured by the spectrometer. Figure 13 shows the additive correction as a function of momentum for this experiment.

Multiple Coulomb Scattering

Multiple Coulomb scattering caused an uncertainty in the measurement of the deuteron angle. The deviation of the true value of θ from the measured value is approximately a gaussian distribution:

$$N \sim \exp\left[-\left(\frac{\theta_{act}-\theta_{meas}}{\Delta\theta}\right)^2\right].$$

The projected angle $\Delta\theta$ is given by the equation[21]:

$$\Delta\theta = \frac{15(\text{Mev})}{PV(\text{Mev})}\sqrt{\frac{L}{L_{rad}}}$$

where P and V are the momentum and velocity of the particle, L is the thickness of the absorber, and L_{rad} is the radiation length of the material. Since the distribution is approximately gaussian, the width resulting from several materials is the square root of the sum of squares of the separate distributions:

$$\Delta\theta = \frac{15(\text{Mev})}{PV(\text{Mev})} \sqrt{\frac{L_i}{(L_{rad})_i}} \quad .$$

This correction shows up in the data in two ways. First it causes an error in the laboratory polar angle due to the scattering material between the target and second spark chamber. Second it causes an error in the measurement of momentum due to scattering of the orbit in passing through the spectrometer. The orbit integration was done using chambers 2, 3, and 4 rather than chambers 1, 2, and 3 because the first combination had less material in the beam.

n+p → γ+d

The differential cross section for n+p → γ+d was obtained from the time reversed photodisintegration reaction γ+d → n+p[22]. The principle of detailed balance was used to transform the cross section to that for n+p → γ+d. Although the cross section for gamma production is about 100 times smaller than that for pion production, there are regions where the kinematics enhances the gamma rate and suppresses the pion rate. Consequently the gamma contamination ranges from 0.02% to 20.0% depending on the kinematic region.

Target Empty Correction

To correct for events coming from the target walls, about six percent of the data were taken with the target empty. These events were binned, and the protons separated in the same way as the target full events. They were normalized using the monitor counters so that the number of incoming neutrons corresponds to that for the target full. This corrections ranges from 4% to 18% for the nine magnet positions.

Deuteron Absorption

Some deuterons were lost in passing through the target

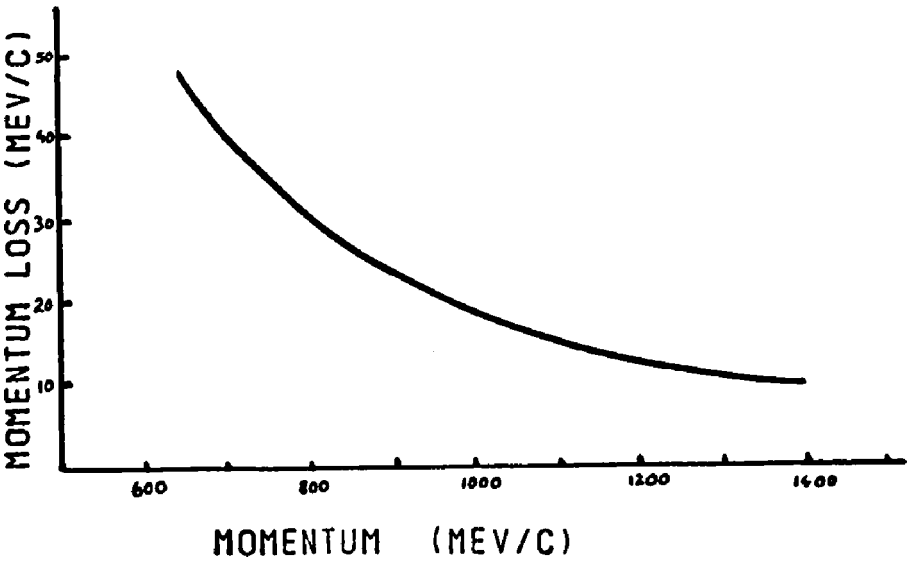


Figure 13: Momentum Loss Vs. Energy of Deuteron

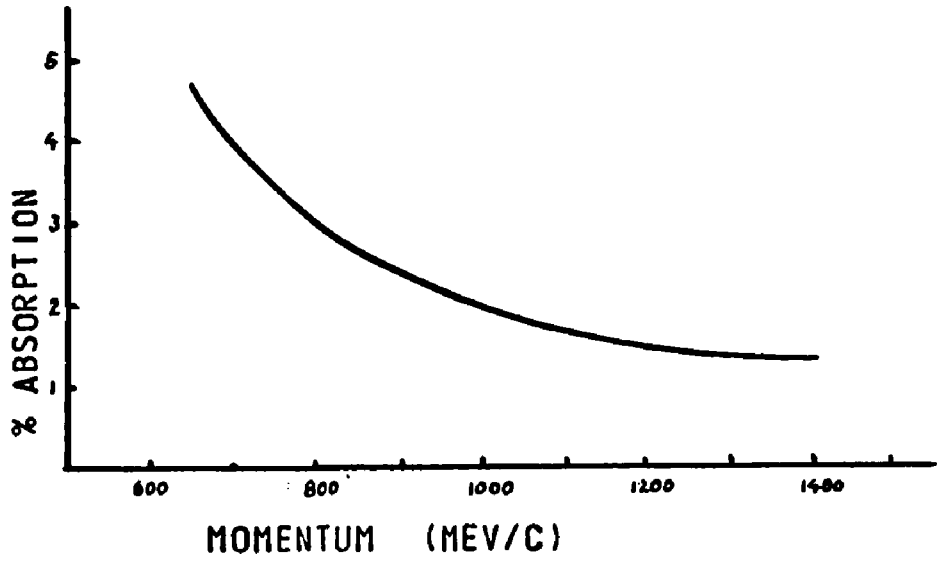


Figure 14: Deuteron Absorption Due to Nuclear Collisions

and spectrometer due to nuclear scattering and absorption. The total cross section for a deuteron-nuclear interaction is strongly momentum dependent for our range of momenta. The deuterons which were lost amount to 4% at 800 Mev/c and 1.4% at 1400 Mev/c. Figure 14 shows the percentage of deuterons lost due to nuclear collisions.

The total cross sections for deuterons on nuclei of atomic number A were obtained by adding the neutron and proton total cross sections multiplied by a screening factor[23]:

$$\sigma(dA) = [\sigma(nA) + \sigma(pA)] \times 0.97 \quad .$$

The total neutron and proton cross sections come from the empirical formula[24]:

$$\sigma(nA) = [(A-Z)\sigma(pp) + Z\,\sigma(np)][1 - 0.155\,A^{.26}]$$

$$\sigma(pA) = [(A-Z)\sigma(np) + Z\,\sigma(pp)][1 - 0.155\,A^{.26}] \quad .$$

The data for $\sigma(np)$ and $\sigma(pp)$ were taken from Reference 24.

The total cross sections for deuterons on nuclei have been measured in our momentum range only at 700 Mev/c[25]. This value is the same as the empirical formulas to about 15% accuracy.

III-H. Cross Section Calculation

The differential cross section is most conveniently expressed as a function of θ and E where θ is the center of mass angle between the deuteron and neutron beam, and E is the incident neutron energy. The raw data can be converted to a differential cross section using the Monte Carlo basic formula:

$$d\sigma(\theta,E) = \frac{N_{expt}(\theta,E)}{N_{gen}(\theta,E,d\sigma_{ext})}\; d\sigma_{est}(\theta,E) \qquad (8)$$

where N_{expt} is the measured number of events in a small bin

centered at θ and E; $d\sigma_{est}$ is an educated estimate of the differential cross section; and N_{gen} is the calculated number of events in the same bin assuming $d\sigma_{est}$ in the calculation. N_{expt} includes a subtraction of the target empty runs. Equation 8 can be iterated - i.e., replace $d\sigma_{est}$ by $d\sigma$ and apply Eq. 8 again. It converges so rapidly that only two iterations were necessary.

The calculation of N_{gen} usually involves a Monte Carlo simulation of the experiment in which the solid angle is also implicitly calculated. In this case it was faster and more accurate to generate events uniformly rather than randomly, and to compute the solid angle separately. (See Sect. III-E.) The determination of N_{gen} proceeded as follows: Events were generated in the center of mass system with θ running from 0° to 180° in 225 steps 0.8° apart, and with E running from threshold to 720 Mev in 120 steps 4 Mev apart. The number of events at each value of θ and E is given by

$$F = d\sigma_{est}(\theta,E) \times Eff(\theta,E) \times D(E) \times M \times Norm \times P$$

where $Eff(\theta,E)$ is the geometric detection efficiency or solid angle as discussed in Sect. III-G. D(E) is the neutron energy distribution normalized to unity. It is discussed in Sect. II-B. M is the number of counts in the beam monitor scaler. Norm is the normalization which relates M to the number of neutrons in the beam. Norm can not be determined independently; it was adjusted to fit the data. P is the number of protons per barn in the target. The events generated in this manner are grouped into bins to form Ngen.

The scattering of both the laboratory polar angle and momentum was folded into F using the scattering distribution in Sect. III-G. The energy loss correction factor was added on. Finally these scaled events were binned in CM coordinates. Compensation for contamination from $d+\gamma$ production was included in N_{gen} by generating events using Eq. 8, except that

$d\sigma_{est}$ was replaced by the cross section for d+λ production.

The threshold for n+p → d+π+π is about 580 MeV. Although our maximum beam energy is above this threshold, the cross section for two pion production at 700 MeV is less than .002 times that for one pion production. Two pion production was therefore neglected.

Also implicity included in the calculation of N_{gen} was its double-valued nature; there are two values of (θ,E) which correspond to each value of the laboratory coordinates (θ_L,P_L). Thus the bounds of a bin in lab space will enclose two distinct CM coordinate regions containing deuterons of two different energies. In Figure 15 the cross-hatched area is the ambiguous kinetic region. In the ambiguous area both N_{expt} and N_{gen} are a composite of the two kinematic regions, so that $d\sigma$ from Eq. 8 is the sum over these two regions, rather than being a direct measurement of the cross section in either. However, most of the data is not ambiguous because in one of the CM regions there are no neutrons of sufficient energy to cause the confusion.

Since there is a large uncertainty in D(E), there will be a correspondingly large uncertainty in the total cross section. A discussion of this uncertainty is given in Section IV-D.

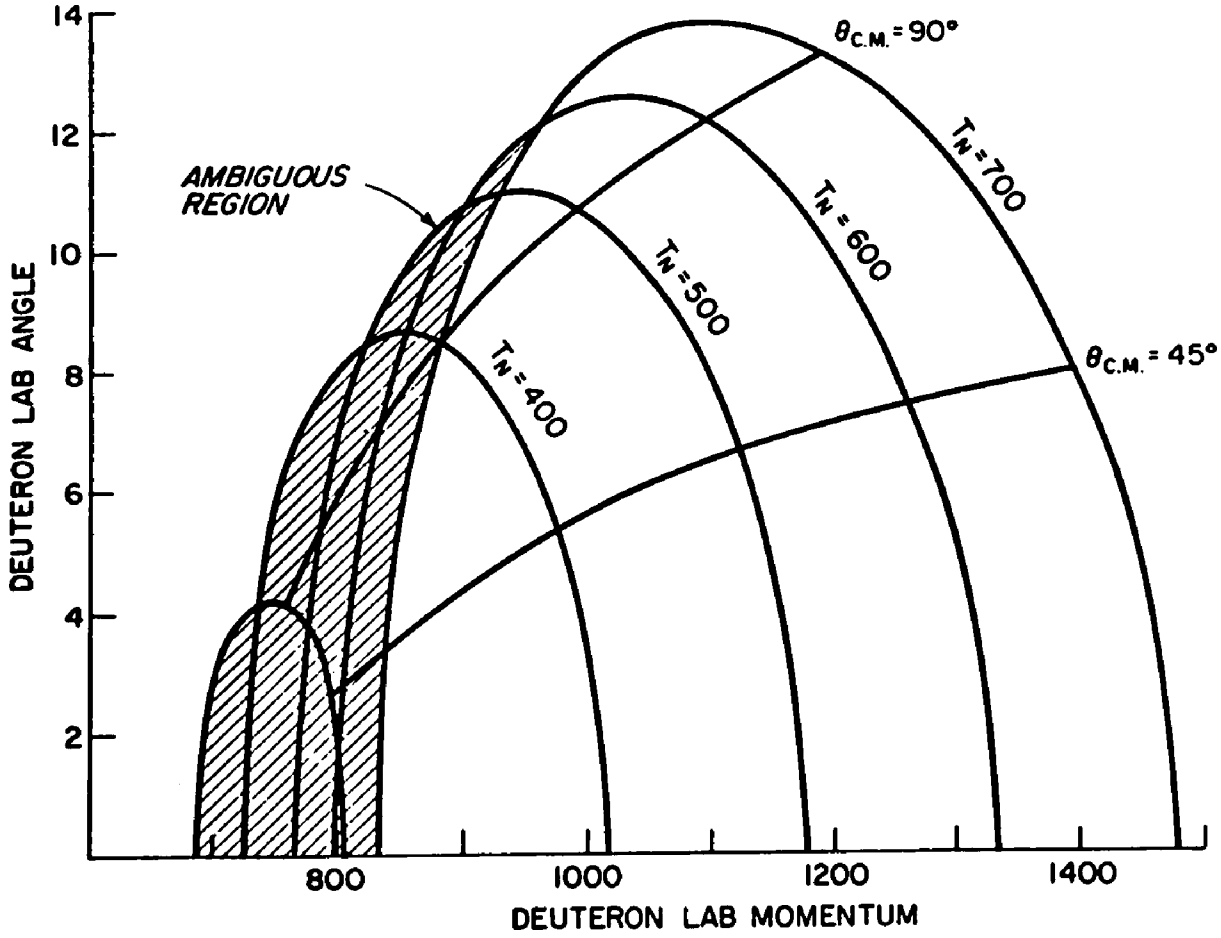


Figure 15: Laboratory Phase Space

IV. RESULTS

IV-A. Cross Section

The cross sections are given in Table 4. The data are in 8 energy bins, 50 Mev wide, from 300 to 700 Mev; and 18 angle bins, 10° wide, from 0° to 180°. Each energy is normalized such that the area is $2\pi \times 1000$. The data are plotted in Figures 16 through 23. The ambiguous points are plotted as open circles. Results from CERN[26] and Princeton[27] are shown as well; however, only a few typical errors are displayed for clarity. The CERN data comes from their measurement of $\pi^+ + d \rightarrow p+p$. It is transformed to conform to $p+p \rightarrow d+\pi^+$ using detailed balance, and then divided by 2 to normalize to $n+p \rightarrow d+\pi^o$. CERN's data covers an angular region from 90° to 180°. It is reflected about 90° and plotted twice. The Princeton results come from a measurement of the same reaction as this experiment. In the plots, our data is normalized to fit the Princeton and CERN results since there is a large uncertainty in our total cross section.

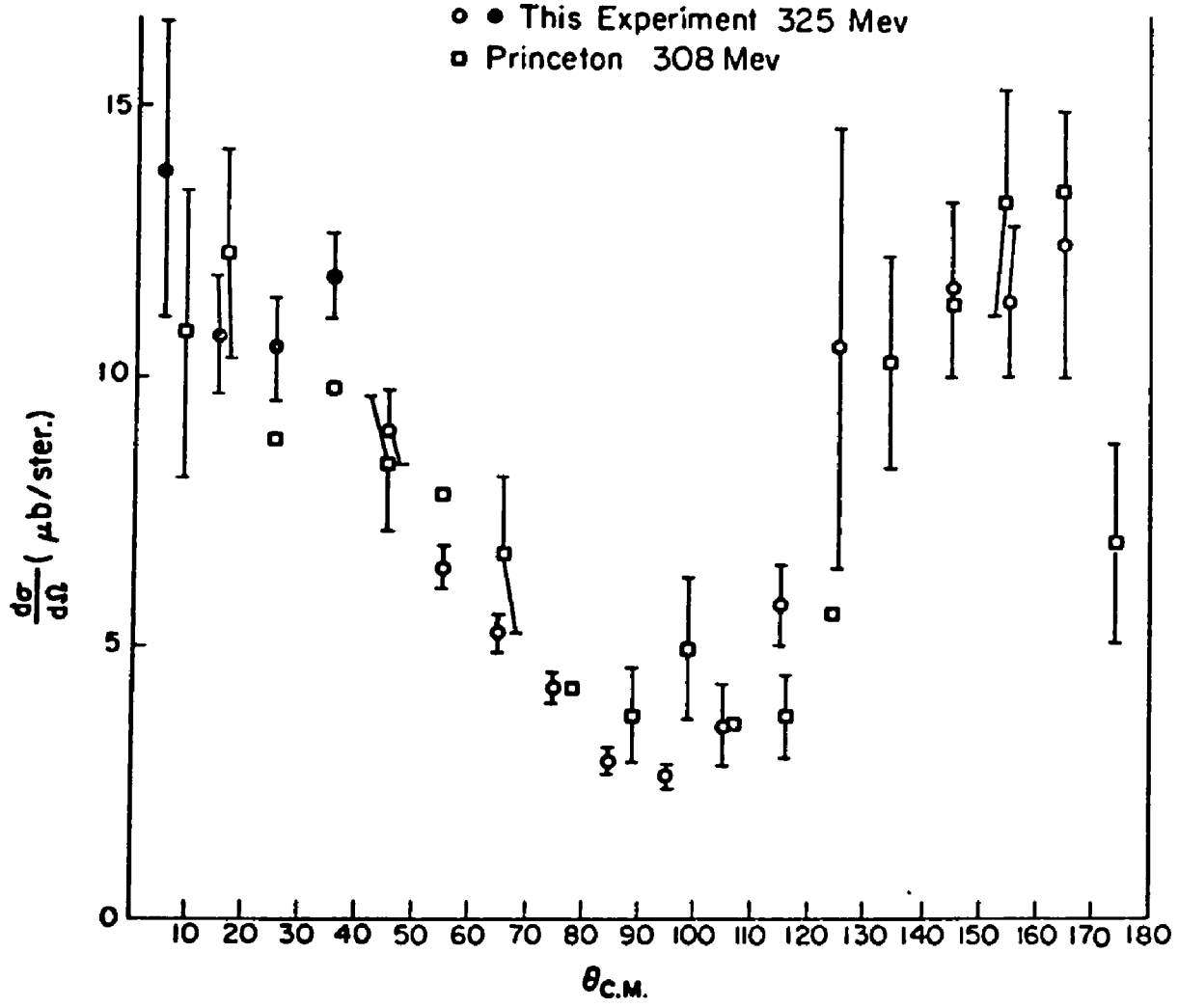
IV-B. Systematic Errors

The alignment of the spark chambers was found to have a maximum inaccuracy of about 1.3 mm. (See Sect. III-C.) This would give a maximum systematic error in the deuteron angle measurement of about 0.05°. The maximum systematic error in the momentum measurement is about 0.5%. The systematic error in the cross section was estimated by varying the lab angle of the deuteron by ±0.05°, and the momentum by 0.5%, and then recomputing the various cross sections. The resulting variations of the cross sections were combined with the statistical errors to obtain the errors quoted in Table 4. The systematic

Table 4

Angular Distributions
Normalized to an Area $2\pi \times 1000$

Angle (CM)	Energy (MeV) 325	375	425	475	525	575	625	675
5°	1046 ±210	1120 ±84	997 ±77	663 ±75	687 ±101	983 ±273	704 ±203	-
15	814 ±81	942 ±41	824 ±27	917 ±33	938 ±38	1097 ±53	804 ±41	835 ±55
25	801 ±75	766 ±50	803 ±33	802 ±35	858 ±32	925 ±34	901 ±52	807 ±55
35	899 ±64	803 ±65	833 ±63	764 ±41	757 ±34	761 ±29	748 ±46	655 ±40
45	684 ±56	767 ±57	653 ±34	612 ±29	637 ±29	667 ±33	660 ±28	636 ±24
55	491 ±34	560 ±39	493 ±25	500 ±25	505 ±24	513 ±25	552 ±23	574 ±18
65	396 ±30	427 ±41	434 ±34	446 ±26	399 ±27	420 ±20	439 ±18	430 ±16
75	319 ±22	330 ±43	314 ±21	333 ±20	316 ±17	270 ±11	281 ±11	317 ±7
85	220 ±18	238 ±18	327 ±29	273 ±16	259 ±12	242 ±10	232 ±10	267 ±7
95	195 ±20	289 ±12	354 ±42	279 ±34	242 ±16	219 ±11	236 ±13	267 ±13
105	269 ±34	265 ±21	322 ±27	377 ±54	352 ±73	320 ±49	317 ±32	344 ±18
115	420 ±60	366 ±48	383 ±37	426 ±24	440 ±28	455 ±65	466 ±67	443 ±34
125	805 ±307	369 ±60	517 ±155	564 ±168	634 ±147	572 ±130	557 ±110	565 ±77
135	-	780 ±364	628 ±82	648 ±87	616 ±51	656 ±41	614 ±43	658 ±66
145	890 ±126	1309 ±348	781 ±85	724 ±74	769 ±57	715 ±44	838 ±88	825 ±109
155	872 ±112	713 ±188	955 ±152	729 ±102	984 ±101	879 ±69	904 ±77	1188 ±320
165	952 ±190	999 ±113	863 ±71	871 ±64	821 ±68	884 ±76	875 ±61	852 ±98
175	-	-	-	1417 ±457	1067 ±244	956 ±118	1048 ±212	757 ±91



Open circles represent points in the ambiguous region.

Figure 16: Differential Cross Section at 325±25 MeV

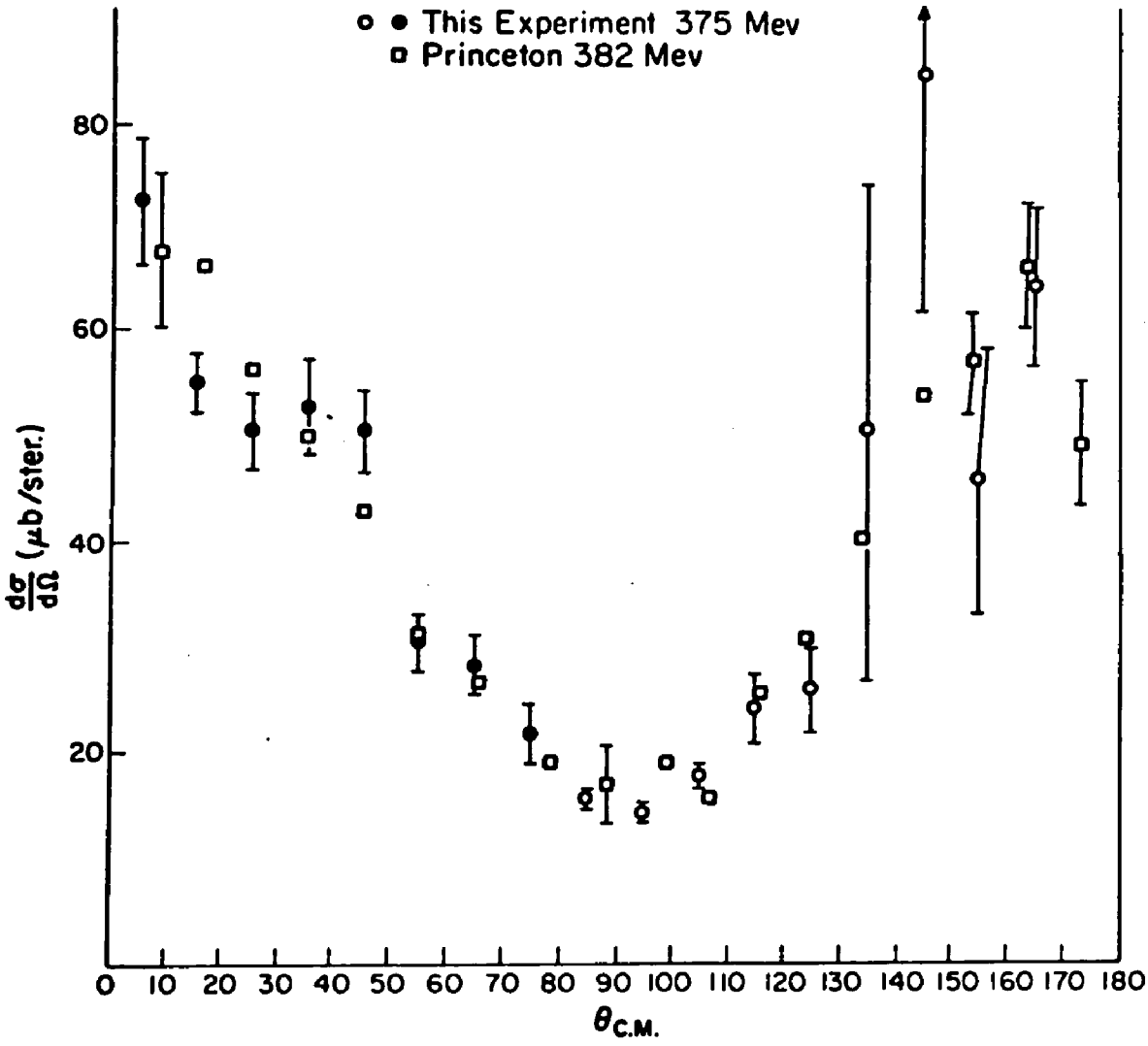


Figure 17: Differential Cross Section at 375±25 MeV

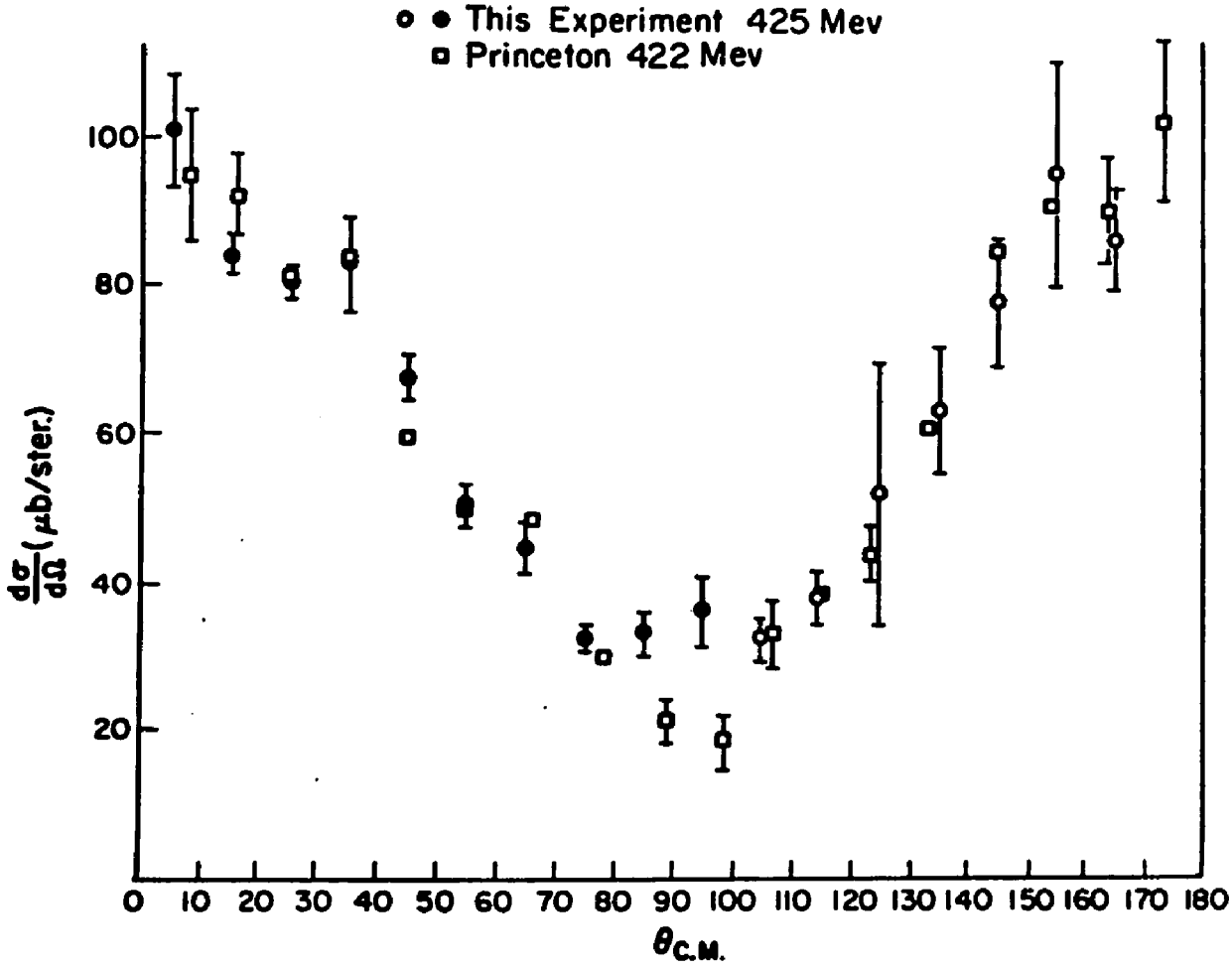


Figure 18: Differential Cross Section at 425±25 MeV

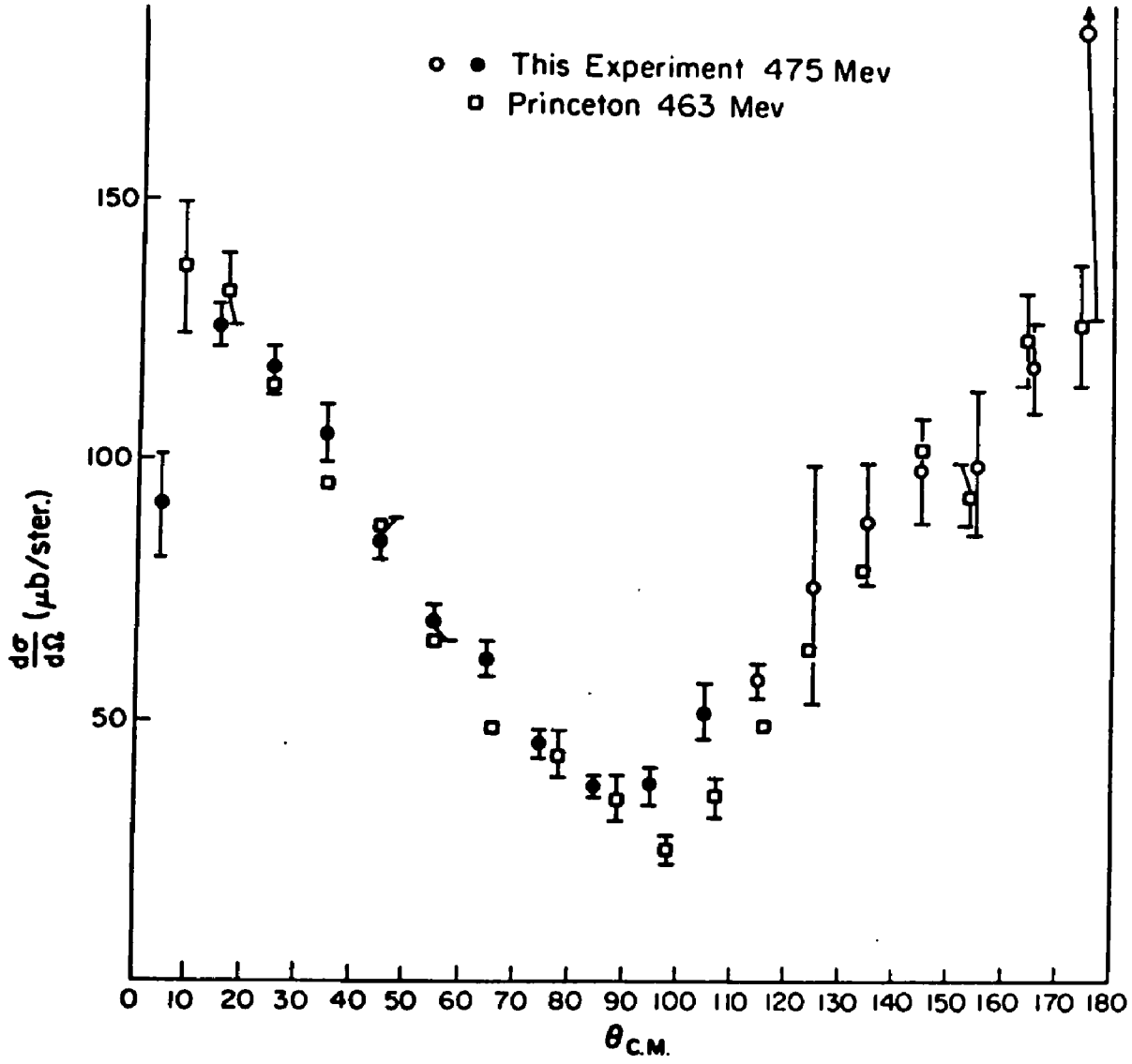


Figure 19: Differential Cross Section at 475±25 MeV

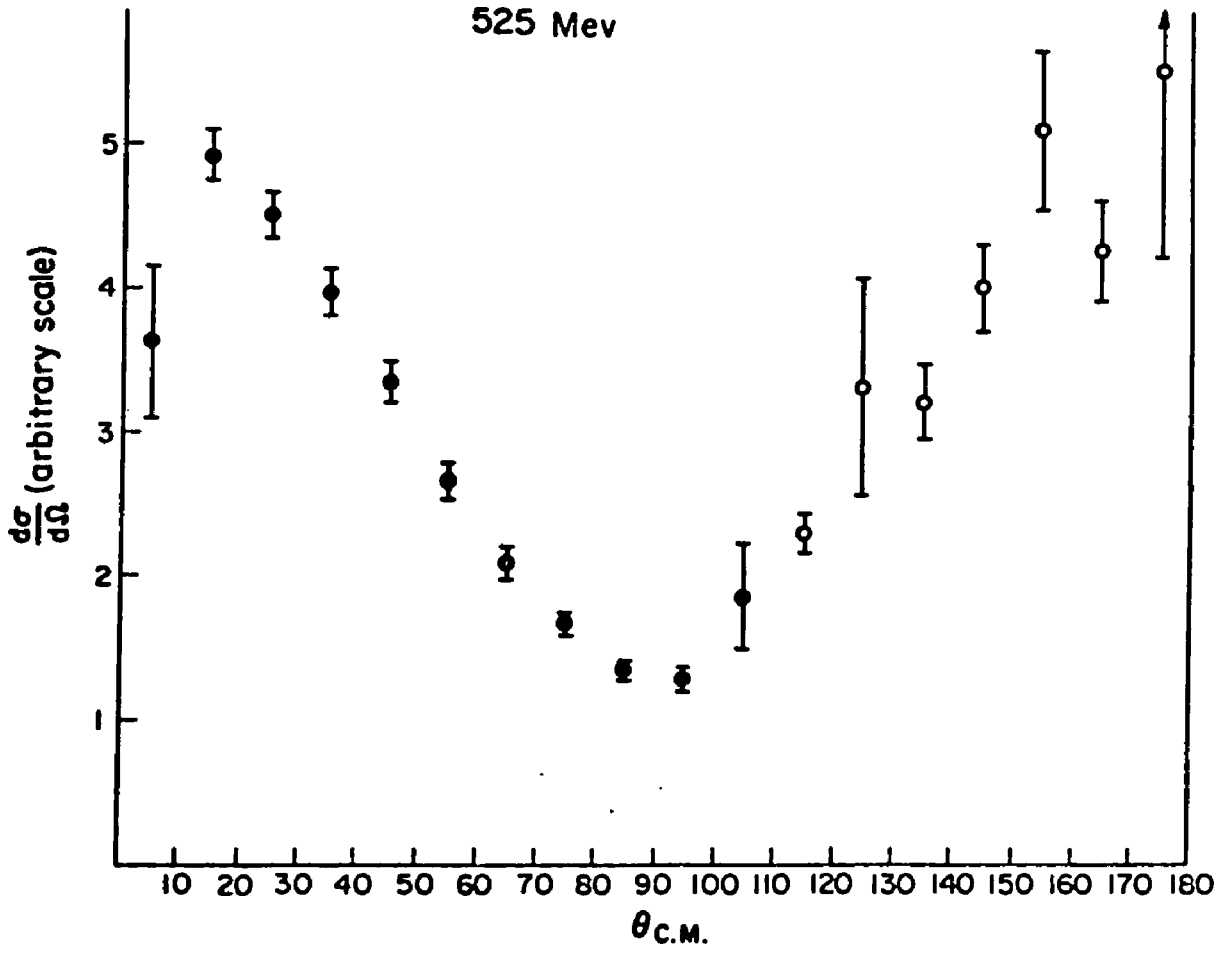


Figure 20: Differential Cross Section at 525±25 MeV

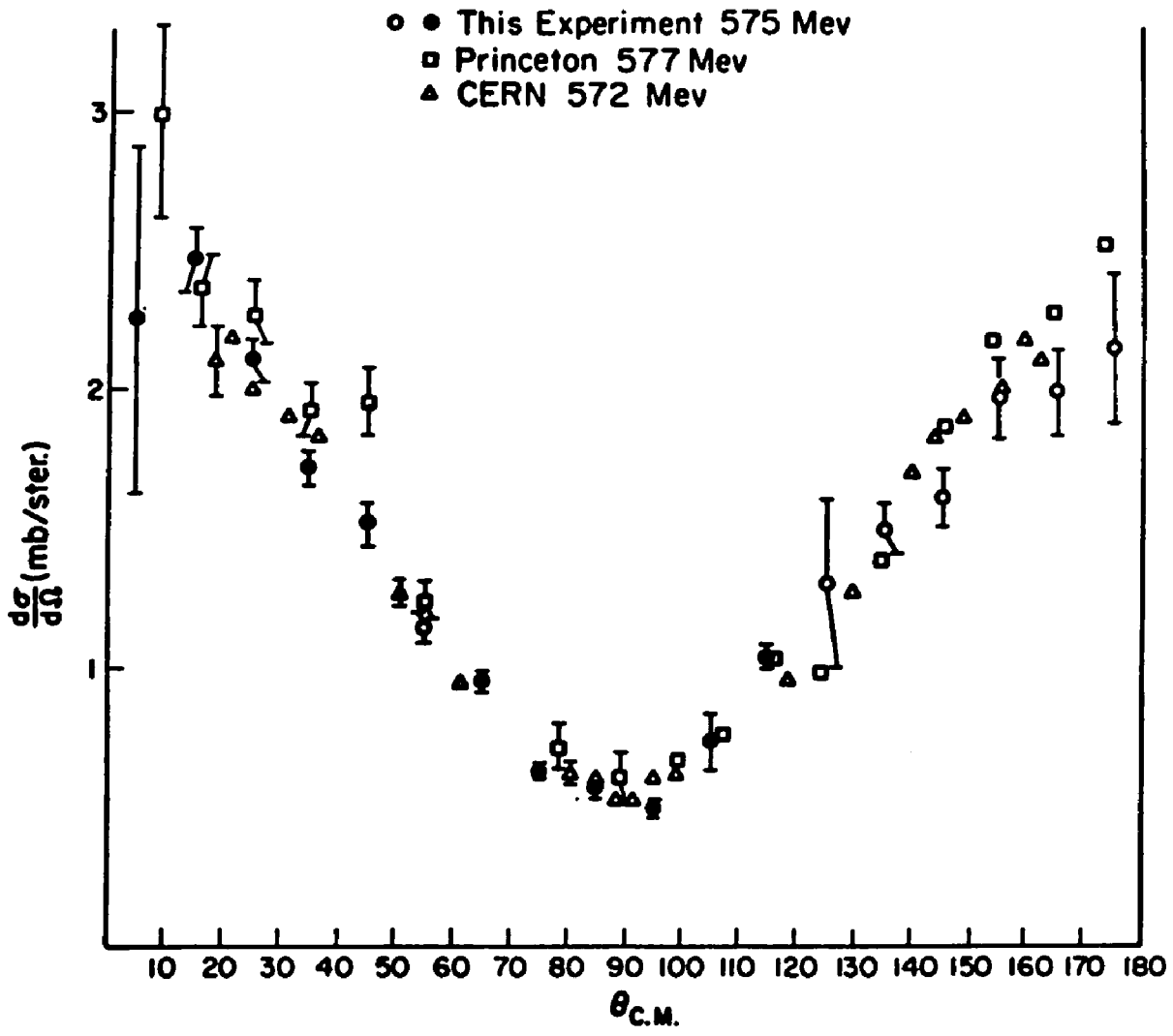


Figure 21: Differential Cross Section at 575±25 MeV

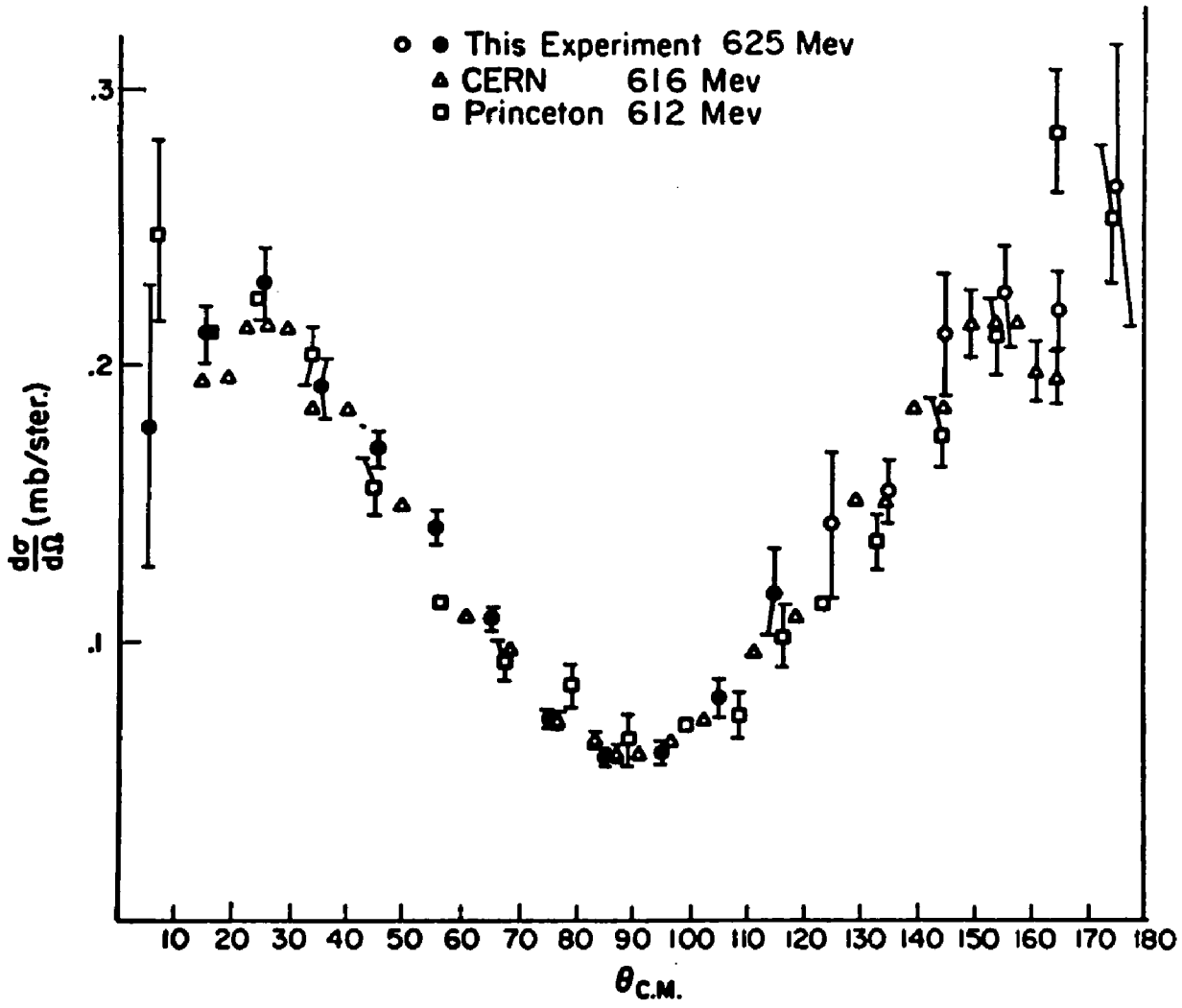


Figure 22: Differential Cross Section at 625±25 MeV

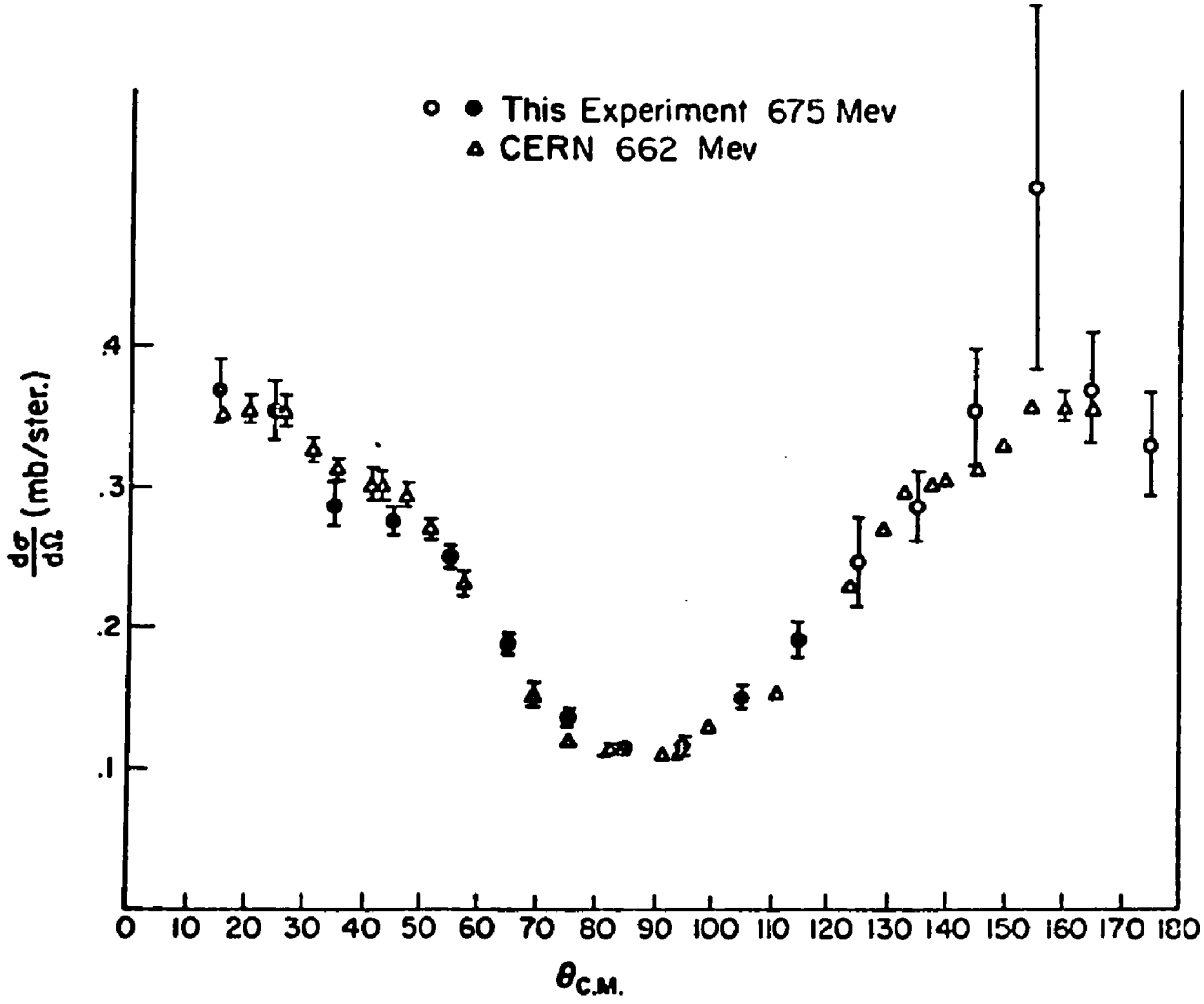


Figure 23: Differential Cross Section at 675±25 MeV

errors are about 1/3 of the statistical errors in the non-ambiguous region, but in the ambiguous region the systematics dominate and cause rather large errors.

IV-C. Coefficients

To conform to the practice of other $N+N \rightleftarrows \pi+d$ experiments, we fit the cross section to the function

$$\sigma(\theta) \sim A + \cos^2\theta + B \cos^4\theta \ . \qquad (9)$$

Our A and B coefficients are plotted as a function of energy in Figure 24 along with the $\pi^+ + d \rightarrow p+p$ results from CERN. There are a number of other experiments measuring the reactions $N+N \rightarrow \pi+d$, but the CERN experiment is the most accurate.

Our cross sections are also fitted to the function:

$$\sigma(\theta) \sim A' + U \cos\theta + \cos^2\theta + B' \cos^4\theta \ . \qquad (10)$$

If isotopic spin invariance is not violated, the coefficient U should vanish. Table 5 shows that U is consistent with zero. Table 5 also gives the values of the other coefficients along with the χ^2 for the fit. The forward-backward asymmetry is defined as

$$A_{fb} = \left[\int_0^{\pi/2} \sigma d\Omega - \int_{\pi/2}^{\pi} \sigma d\Omega \right] / \left[\int_0^{\pi/2} \sigma d\Omega + \int_{\pi/2}^{\pi} \sigma d\Omega \right]$$

and is shown in Fig. 24. A_{fb} serves as an important measure of the violating amplitudes, and is discussed in Sect. IV-F.

A fit to the function

$$\sigma(\theta) \sim A' + \cos^2\theta$$

gives a much larger χ^2 than that for Eq. 9. Thus the B coefficient is necessary for a fit to this experiment.

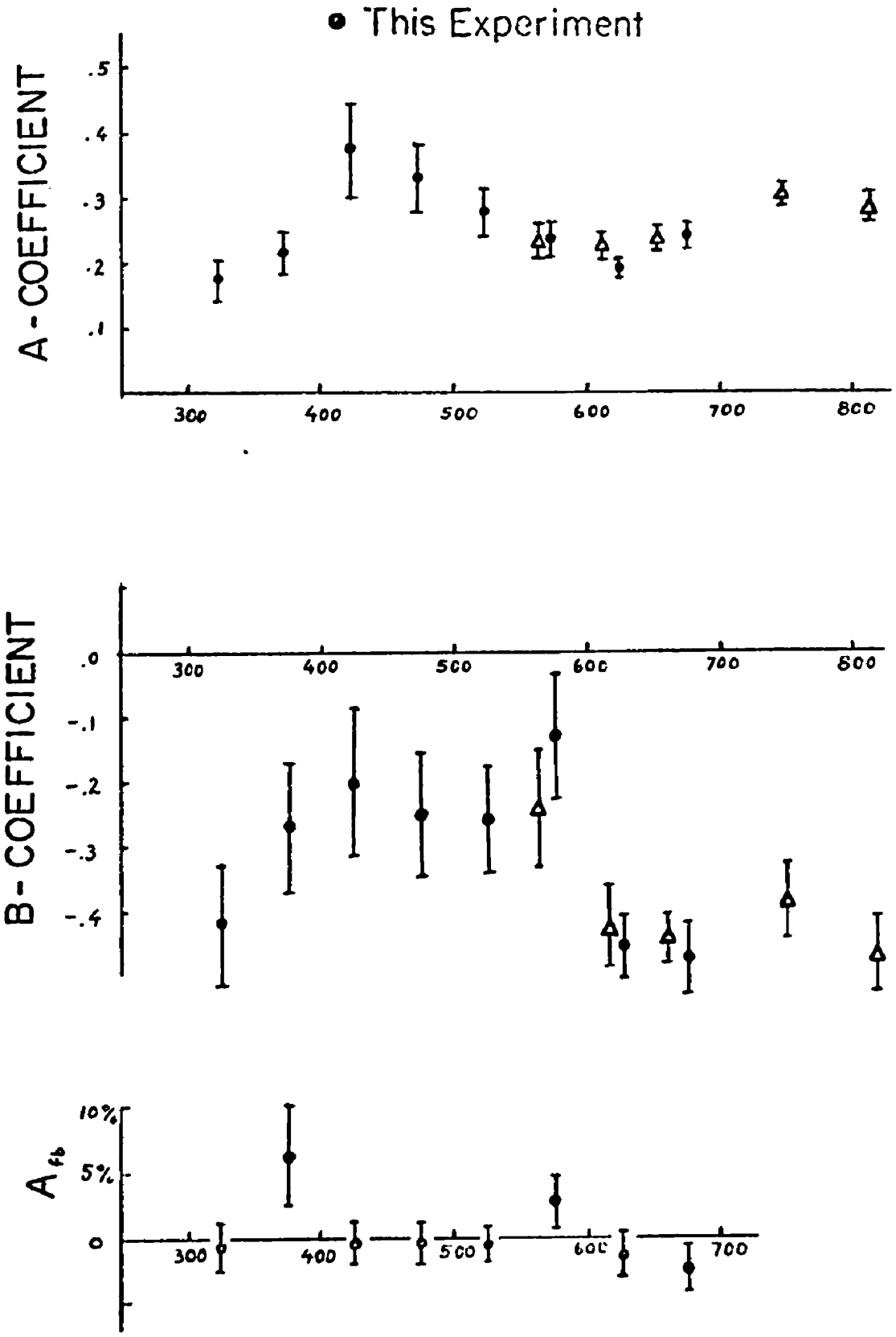


Figure 24: Coefficients

Table 5

Coefficients

Energy (MeV)	A	B	χ^2 per deg. of freedom	U	A_{fb}
325	.171±.031	-.412±.094	13.6/14	-.007±.027	-.8±2.1
375	.209±.033	-.263±.099	25.5/15	+.066±.038	6.5±3.8
425	.379±.076	-.199±.122	17.5/15	-.007±.027	-.5±1.9
475	.335±.052	-.254±.094	19.8/17	-.006±.022	-.5±1.8
525	.274±.034	-.253±.084	15.5/16	-.007±.019	-.6±1.6
575	.242±.028	-.130±.097	20.7/16	+.033±.022	2.9±1.9
625	.189±.018	-.452±.051	15.0/16	-.012±.014	-1.4±1.6
675	.247±.021	-.474±.057	13.1/15	-.023±.016	-2.4±1.7

IV-D. Comparison with Other Experiments

As shown in Section I-C, the invariance of the strong force with respect to the third component of isospin leads to the result that the angular distribution of $p+p \rightarrow \pi^+ + d$ and $n+p \rightarrow \pi^o + d$ are the same.

The CERN $\pi^+ + d \rightarrow p+p$ experiment is the only $N+N \rightleftarrows \pi+d$ experiment which has comparable accuracy to our experiment. There is very good agreement for our results with CERN's for both the A and B coefficients as shown in Fig. 24. Our data is also consistent with all other $N+N \rightleftarrows \pi+d$ experiments though the accuracies of their B coefficients are poor enough that this is not a very fruitful comparison. A summary of these other experiments can be found in Ref. 26.

The agreement of the coefficients was studied at the three energies for which the CERN experiment and ours overlap. Good agreement was found. Table 6 gives the maximum probability that a violation occurs with a 90% confidence level.

Table 6
Maximum Violation with 90% Confidence Level

Energy (MeV)	Violation in A	Violation in B
575	<9.5%	<6.3%
625	<8.5%	<4.3%
675	<7.8%	<3.5%

The Princeton experiment has measured the angular distribution for the same reaction as our experiment in the same energy range. Their systematic errors are too large to allow them to detect the B coefficient. Their measurement of the asymmetry A_{fb} is consistent with zero, but their inaccuracy is over four times larger than ours.

IV-E. Total Cross Section

In order to measure the total cross section, we must know the energy distribution of the neutron beam. The energy distribution was measured using the $n+p \rightarrow \gamma+d$ experiment as discussed in Sect. II-B. The distribution in Fig. 2 does not show the errors which range from 40% at low energies to 20% at higher energies. This will cause an equally large error in our measurement of the total cross section.

The total cross section is shown in Figure 25 along with the total cross section for $p+p \rightarrow \pi^{+}+d$[27]. The cross sections are not plotted as lines, but are indicated by bands which show the uncertainty in the measurement. The cross sections are consistent, but the uncertainties are too large for the comparison to be of much value.

IV-F. Comparison with Theory

The theory of pionic disintegration of the deuteron by

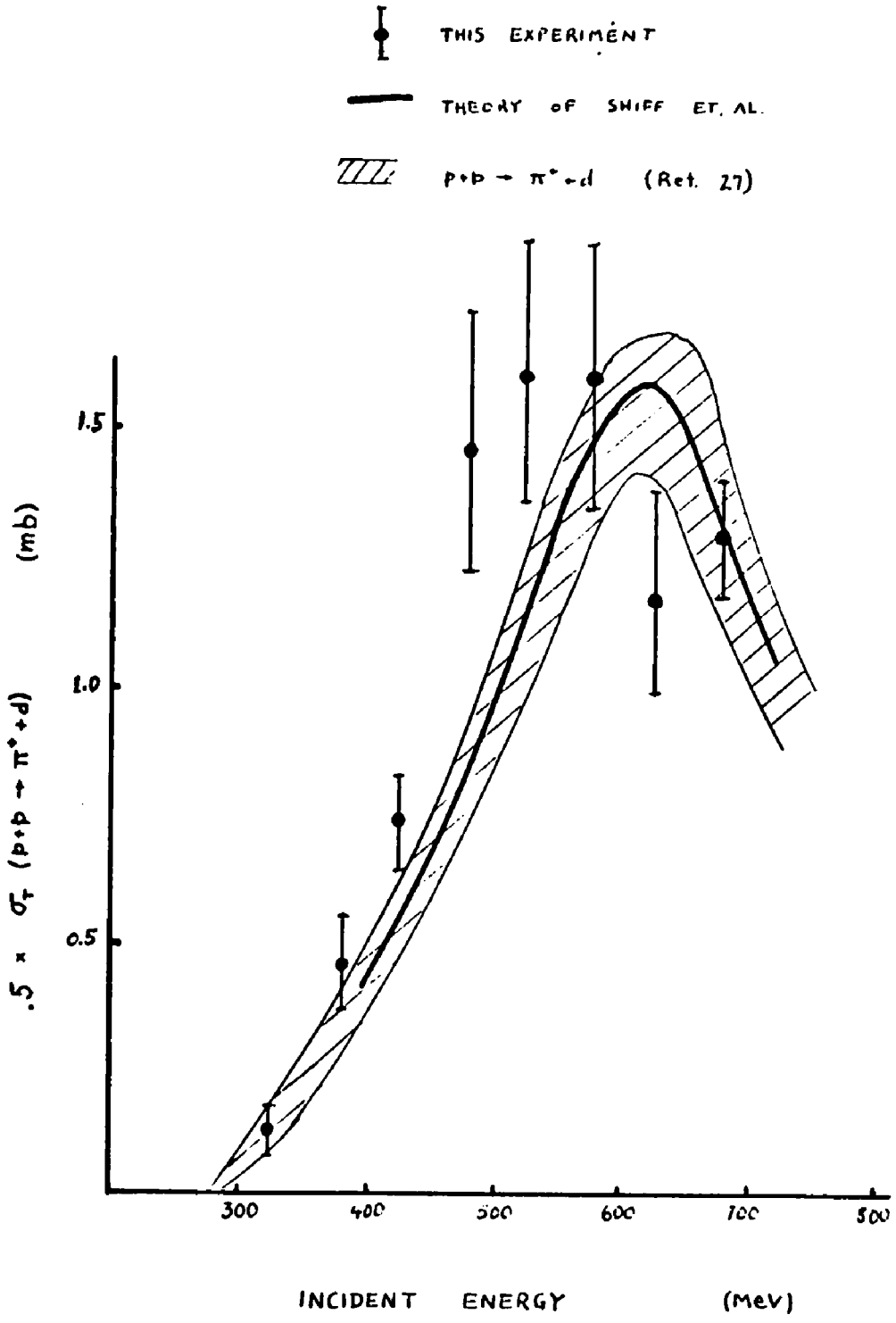


Figure 25: Total Cross Section

D. Shiff and J. Tran Thanh Van[9] is the only theory which predicts the B coefficients. Rather than giving their results in terms of the A and B coefficients, they plot their derived angular distributions at several energies. The coefficients can be otained by fitting Eq. 9 to their plots. The results of this fit are given in Table 7.

Table 7
Coefficients of Shiff et. al.

Energy (MeV)	A	B
460	.87	.66
572	.61	.50
633	.54	.47
690	.49	.43
745	.45	.40

Our experimental results have the same magnitude, but the opposite sign for the B coefficients. No attempt will be made here to try and explain this discrepancy because the significance of the B coefficients is obscurely imbedded in the theory - they result primarily from an interference of higher order partial waves with the dominant transition.

The theory is much more successful in deriving the total cross section. This theory and the experimental measurements of the total cross section are shown in Figure 25.

If isospin invariance is violated, it has been shown[27] that the important violating amplitudes (transitions with I=0 to I=1) would be

$$f = ({}^1P_3 \rightarrow {}^3S_1)$$
$$g = ({}^1P_1 \rightarrow {}^3D_1)$$
$$h = ({}^1F_3 \rightarrow {}^3D_3)$$

These transitions give rise to antisymmetric terms in the angular distribution. Moreover, the ratio of the violating to the nonviolating amplitudes can be given by:

$$f = 2^{-1/2}A_{fb} \; ; \quad g = 4A_{fb} \; ; \quad h = 6^{-1/2}A_{fb} \; .$$

Since the average value of our measurement of A_{fb} is only $-.36\pm.66\%$, we have set a tight upper limit on the total isospin violating amplitude. (See Sect. I-C.) To the extent that A_{fb} is a measure of the ratio of the violating to the nonviolating amplitude, this limit is about 1%.

V. CONCLUSIONS

Isospin invariance has been tested in several experiments involving pions and light nuclei. (See Sect. I-D for a summary.) These tests show that isospin is conserved to at least 5%. The recent experiment at Princeton[27] results in a forward-backward asymmetry of 1±3% in the angular distribution of the reaction $n+p \rightarrow \pi^{o}+d$. Our results show an average asymmetry of 0.36±0.66% in the same reaction.

Our angular distribution agrees well with all other $N+N \rightleftarrows \pi+d$ experiments. In fitting the cross section to the formula

$$\sigma(\theta) \sim A + \cos^2\theta + B \cos^4\theta$$

we and CERN[26] find consistently negative values for B with a sharp negative drop above 600 Mev. The angular distributions for these two experiments are the same within ~9% uncertainty. Evidence from the forward-backward asymmetry shows that transitions which no not conserve isospin do not occur to within about 1.0% accuracy - the level at which electromagnetic violations might be expected to occur.

LIST OF REFERENCES

1. B. Schrock, et al. UCLRL 19350 (1969).
2. J. Cerny, Ann. Rev. of Nucl. Sci., 18, 27 (1968).
3. A.A. Carter, et al., Phys. Rev., 168, 1457 (1968).
4. W. Galbraith, et al., Phys. Rev., 138, B913 (1965).
5. J.A. Poirier & M. Pripstein, Phys. Rev., 130, 1171 (1963).
6. K.R. Greider, Phys. Rev., 122, 1919 (1961).
7. A.V. Crewe, et al., Phys. Rev. Letters, 2, 114 (1959).
8. D. Hartig, et al., Phys. Rev., 119, 1716 (1960).
9. D. Shiff & J. Tran Than Van, Nucl. Phys, B5, 671 (1968).
10. V.S. Kiselev, et al, JETP, 35, 812 (1958).
11. W.A. Wenzel, Am. Rev. of Nucl. Sci., 14, (1964).
12. F.A. Kirsten, et al., UCLRL 16539 (1965).
13. V. Perez-Mendez, et al., Nucl. Inst. and Meth., 46, 197 (1967).
14. Q. Kerns, UCLRL 10887 (1963).
15. Chronetics Inc., 500 Nuber Ave., Mt. Vernon, New York.
16. R. Hinkins, T. Schaefer, L. Wilson, private communication, (not published).
17. B. Rust, et al., ACM, 9, no. 5, 381 (1965).
18. Program "LINERR" by R. Hinkins, private communication.
19. H. Bichsel, UCLRL 17538 (1967).
20. H.A. Bethe, Quantenmechanik der Ein-und Zwei Elektronen-probleme, in "Handbuch der Physik," Vol. 24-I, 2nd ed., (Julius Springer Verlag, Berlin, 1933).
21. N. Barash-Schmidt, et.al., UCLRL 8030 (1968).
22. R.L. Anderson, et al., Phys. Rev. Letters, 22, 651 (1969).
23. E. Parker, U of M Thesis, Tech. Report 03028-3-T, (1970).
24. R. Wilson, The Nucleon-Nucleon Interaction, Interscience Publ. (1963).
25. G.P. Millburn, Phys. Rev., 95, no. 5, 1268 (1954).
26. C. Richard-Serre, CERN 68-40 (1968).
27. D.F. Bartlett, et al., Phys. Rev. D, 1, no. 7, (1970).